SEMI-TAILLESS AIRCRAFT CONCEPT WITH VARIABLE CANT STABILIZERS APPLIED TO SMALL UAVS

A Thesis by

Kevin Hagen

Bachelor of Science in Aerospace Engineering, Wichita State University, 2017

Submitted to the Department of Aerospace Engineering
and the faculty of the Graduate School of
Wichita State University
in partial fulfillment of
the requirements for the degree of
Master of Science

May 2019

SEMI-TAILLESS AIRCRAFT CONCEPT WITH VARIABLE CANT STABILIZERS APPLIED TO SMALL UAVS

The following faculty members have examined the final copy of this thesis for form and content, and recommend that it be accepted in partial fulfillment of the requirement for the degree of Master of Science, with a major in Aerospace Engineering.

L. Scott Miller, Committee Chair

James Steck, Committee Member

Thomas DeLillo, Committee Member

ACKNOWLEDGMENTS

There are too many people who deserves thanks for their support during the completion of this thesis to list in these acknowledgements but know that even if not specifically mentioned your support is still greatly appreciated.

Thanks to my committee members, Dr. James Steck and Dr. Thomas DeLillo, for the taking the time to read and review my thesis, and who's suggestions improved the final product.

I want to thank my family for their support, and for their encouragement of my curiosity. My parents, who allowed their children to take apart, and usually destroy, their stuff in the pursuit of learning. I also want to thank my brother, Brian, who participated in the destruction, and who's talent and skill has always pushed me to improve my own abilities.

To my coworkers, Kayle, Colton, and Linda, for their assistance in building and testing. Yrithu Pillay, for his support during flight testing, as well as taking pictures and videos. Vijay Matheswaran, who's tireless assistance in wind tunnel and flight testing improved the results of the thesis, and for patiently listening when I needed to work out ideas.

A special thanks goes to Jon Mowery, for taking time away from his family to try to get my airplane to fly. Without his exceptional piloting ability, I likely would not have had the confidence to take on this topic, and his feedback and advice was instrumental in success flights.

Finally, I want to extend my deepest gratitude to my advisor and mentor, Dr. L. Scott Miller. His tireless support, guidance, and encouragement, not only academically but also personally, has enabled many of my life's successes.

ABSTRACT

In recent years the use of small UAVs (<5lbs) has grown rapidly. While fundamentally the same as large aircraft, differences in requirements, payloads, and cost allow for a greater number of viable concepts. Many new concepts have been proposed however, old concepts that were never adopted for large aircraft may be viable for small UAVs. One such concept is a semi-tailless concept proposed by Blohm & Voss in 1944. This concept placed the stabilizer surfaces outboard and aft of the wing tips of a highly swept main wing. This allowed for the empennage to be removed, resulting in a reduction of empty weight and wetted area, improving a number of performance parameters. Applying this concept to small UAVs potentially mitigate the downsides, while providing additional opportunities. Specifically, varying the stabilizer cant angle to provide control and improve performance. Using the basic geometry developed by Blohm & Voss, trade studies were done to determine the stabilizer cant angle effect. A simple analytical model was used to identify the key parameters affecting control. The configuration was then modeled with a vortex lattice solver to predict performance. Wind tunnel and flight testing was performed to validate predictions and provide pilot feedback on the aircraft's behavior. It was found that the variable cant stabilizers do allow sufficient control for most flight regimes, and small increases in performance are possible. The results show that the concept is viable for application to small UAVs.

TABLE OF CONTENTS

TABLE OF CONTENTS (continued)

LIST OF TABLES

LIST OF FIGURES

LIST OF FIGURES (continued)

LIST OF FIGURES (continued)

Figure Page

LIST OF ABBREVIATIONS

AC	Aerodynamic Center
B&V	Blohm and Voss
CG	Center of Gravity
L/D	Lift-to-Drag Ratio
LE	Leading Edge
LEX	Leading-edge Extension
LSWT	Low Speed Wind Tunnel
MAC	Mean Aerodynamic Chord
NACA	National Advisory Committee on Aeronautics
NP	Neutral Point
OHS	Outboard Horizontal Stabilizer
SAE	Society of Automotive Engineers
SAS	Stability Augmentation System
SM	Static Margin
UAVs	Unmanned Aerial Vehicles

LIST OF SYMBOLS

α	Aircraft Angle of Attack
α_S	Stabilizer Local Angle of Attack
β	Aircraft Sideslip Angle
C_D	Total Aircraft Drag Coefficient
C_{D_0}	Parasite Drag of Aircraft
C_{D_α}	Variation of Aircraft Drag with Angle of Attack
$C_{D_{\delta_e}}$	Variation of Aircraft Drag with Elevator Deflection
C_{D_q}	Variation of Aircraft Drag with Pitch Rate
$c_{l_{max}}$	Maximum Lift Coefficient for Airfoil
C_l	Rolling Moment Coefficient of Aircraft
C_{l_β}	Variation of Aircraft Rolling Moment with Sideslip Angle
$C_{l_{\delta_a}}$	Variation of Aircraft Rolling Moment with Aileron
C_{l_p}	Variation of Aircraft Rolling Moment with Roll Rate
C_{l_r}	Variation of Aircraft Rolling Moment with Yaw Rate
$C_{L_{0_W}}$	Lift at Zero Angle of Attack for Wing
C_{L_α}	Variation Of Airplane Lift Coefficient With Angle Of Attack
$C_{L_{\alpha_S}}$	Variation Of Stabilizer Lift Coefficient With Angle Of Attack
$C_{L_{\alpha_W}}$	Variation Of Wing Lift Coefficient With Angle Of Attack
$C_{L_{\delta_e}}$	Variation of Aircraft Lift with Elevator Deflection
$C_{L_{max}}$	Maximum Lift Coefficient for Aircraft
C_{L_q}	Variation of Aircraft Lift with Pitch Rate

C_M	Pitching Moment Coefficient of Aircraft
C_{M_α}	Variation of Aircraft Pitching Moment with Angle of Attack
$C_{M_{\delta_e}}$	Variation of Aircraft Pitching with Elevator Deflection
$C_{M_{W_{\delta_f}}}$	Variation of Wing Pitching Moment Coefficient With Flap Deflection
C_{M_q}	Variation of Aircraft Pitching with Pitch Rate
C_n	Yawing Moment Coefficient for Aircraft
C_{n_β}	Variation of Aircraft Yawing Moment with Sideslip Angle
$C_{n_{\beta_W}}$	Yawing Moment Variation of Wing with Sideslip Angle
$C_{n_{\delta_a}}$	Variation of Aircraft Yawing Moment with Aileron
C_{n_p}	Variation of Aircraft Yawing Moment with Roll Rate
C_{n_r}	Variation of Aircraft Yawing Moment with Yaw Rate
C_Y	Side-Force Coefficient for Aircraft
C_{Y_β}	Variation of Aircraft Side-Force with Sideslip Angle
$C_{Y_{\beta_W}}$	Side-Force Variation of Wing with Sideslip Angle
$C_{Y_{\delta_a}}$	Variation of Aircraft Side-Force with Aileron
C_{Y_p}	Variation of Aircraft Side-Force with Roll Rate
C_{Y_r}	Variation of Aircraft Side-Force with Yaw Rate
δ_e	Elevator Deflection
δ_f	Flap Deflection Angle
$\Delta\alpha_{0_L}$	Change in Angle of Zero Lift

LIST OF SYMBOLS (continued)

F_S	Stabilizer Aerodynamic Force
γ_S	Stabilizer Cant Angle
i_S	Stabilizer Incidence Angle
K_f	Plain Flap Correction Factor
L	Total Aircraft Lift
L_A	Rolling Moment of Aircraft
L_S	Stabilizer Lift
L_W	Lift Due to Wing
M	Pitching Moment of Aircraft
M_{ac_W}	Pitching Moment of Wing About Aerodynamic Center
M_{δ_f}	Pitching Moment due to Flap Deflection
N_A	Total Yawing Moment of Aircraft
N_{A_W}	Yawing Moment of Wing
q_∞	Dynamic Pressure
S_S	Stabilizer Area
$S_{flapped}$	Area of Wing with Flaps
S_W	Area of Wing
t_S	Stabilizer Toe Angle
V_∞	Aircraft Airspeed
x_{ac_S}	X-Location of Stabilizer Aerodynamic Center
x_{ac_W}	X-Location of Wing Aerodynamic Center
x_{cg}	X-Location of Center of Gravity

LIST OF SYMBOLS (continued)

$\bar{x}_{ac_S}$	X-Location of Aerodynamic Center of Stabilizer as Fraction of MAC
$\bar{x}_{ac_W}$	X-Location of Aerodynamic Center of Wing as Fraction of MAC
$\bar{x}_{cg}$	X-Location of Center of Gravity as Fraction of MAC
$\bar{x}_{cp}$	X-Location of Center of Pressure of Flaps as Fraction of MAC
y_{ac_R}	Y-Location of Aerodynamic Center of Right Stabilizer
y_{ac_L}	Y-Location of Aerodynamic Center of Left Stabilizer
y_{AR}	Stabilizer Axis of Rotation Y-Location
Y_A	Total Side-Force of Aircraft
Y_{A_W}	Side-Force Due to Wing
Y_S	Stabilizer Side force
$\overline{Y_S}$	Spanwise Location of Stabilizer MAC
z_{ac_L}	Z-Location of Aerodynamic Center of Left Stabilizer
z_{ac_R}	Z-Location of Aerodynamic Center of Right Stabilizer
z_{AR}	Stabilizer Axis of Rotation Z-Location

CHAPTER 1

INTRODUCTION

Since mankind first started dreaming of taking to the sky many different ideas of what a flying machine should be have been suggested. Although many concepts have been proposed not all of them have ever been built and flown. While a portion of the unflown concepts are likely not viable, a large number of viable concepts have been discarded; deemed either too risky or not beneficial enough, they have been forgotten. However, growth in the use of small (<5lbs), low-Reynolds number unmanned aerial vehicles (UAVs) may provide opportunities to apply riskier, but beneficial, concepts. A concept that has a number of possible benefits but was never adopted is the Blohm & Voss semi-tailless concept, proposed in late 1944. This concept places the stabilizers outboard and aft of the wing tips, eliminating the need for an empennage, reducing both the empty weight and the wetted area. Although the original concept had the stabilizers mounted at a fixed cant angle relative to the wing, varying this angle in flight may provide benefits for both control and performance.

1.1 Small UAVs

In the last decade the use of small UAVs has exploded and are being applied to a variety of missions including military, surveillance, surveying, agriculture, civil engineering, ecological, emergency relief, package delivery, flight in the Martian atmosphere, and many more. While fundamentally the same as full-scale aircraft, differences in requirements, payloads, construction methods, and cost has led to greater willingness to experiment with unique configurations.

While all of these factors play a role, low-cost is the primary driver of experimentation. Developing a full-scale aircraft is an expensive proposition; large teams of engineers are required to design, construct, test, and certify an aircraft, and the process takes years to complete. Small

UAVs can be made relatively cheaply and quickly; a small team of engineers can develop and test a design in just a few months. This allows companies to be more willing to experiment and test risky concepts. Small UAVs can also be made to suit much more specific missions, and developing a robust design is potentially not as critical.

Structural scaling also plays a role in the design of small UAVs, with differences in the methods and materials used. While some UAVs are constructed using a semi-monocoque scheme in much the same way as full-scale aircraft, this is less common. Small UAVs do not need to carry fuel in the wings and they can be made with a solid core. Typically, foam is used for the core, and then a load bearing skin bonded onto the surface. This method has a number of benefits; it is simple to design, fast and easy to construct, requires fewer parts, and is robust. The wings also tend to be very stiff, especially in torsion. These differences can make some concepts that would not be possible on full-scale aircraft applicable to small UAVs.

1.2 Semi-Tailless Configuration

Starting in 1944 Blohm & Voss (B&V) proposed the first in a series of fighter/interceptor designs that utilized a semi-tailless configuration [1]. Sometimes also referred to as outboard-horizontal-stabilizers (OHS), this design places the main stabilizer surfaces outboard and aft of the wing tips. This stabilizer placement took advantage of the highly swept wings that were required for high-speed flight brought about by turbojet development. The wing tips of these swept wings were shifted far enough aft to provide sufficient moment arm for the stabilizers, which eliminated the need for an empennage. A diagram showing how a traditional straight-wing configuration could be converted into a semi-tailless configuration is shown in Figure 1.

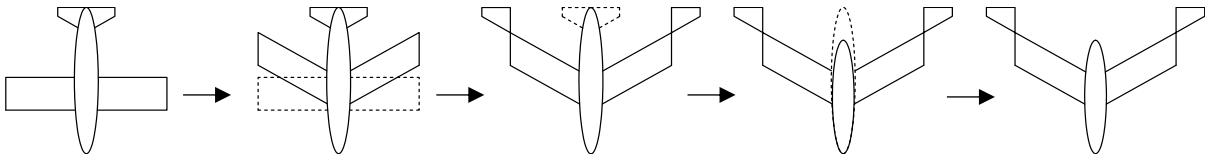

Figure 1. Transformation from conventional to semi-tailless configuration.

Eliminating the empennage leads to a reduction in weight and wetted area which helps to maximize flight speed, a main goal of the B&V concept. The location on the wing tip also places the stabilizers in a much better flow field. When mounted on an empennage the stabilizers are in a region of downwash and reduced velocities; but outboard of the wing tips the stabilizers are in a region of upwash and no velocity deficit. This allows the stabilizers to be made smaller than if they were mounted on an empennage, further reducing weight and wetted area [2].

Besides maximizing speed, the configuration provides additional benefits. With no empennage the aircraft can utilize a pusher configuration, allowing an unobstructed view for the pilot and also allowed armaments to be placed in the aircraft nose rather than the wing. It is also interesting to note how the designs fit the environment they were created in. Late in 1944 there was a shortage of materials in Germany, and the design requires less materials than a conventional design. All designs also utilize simple wings with no taper or twist, which would make them easy and quick to build [3]. These features also make the design well suited to small UAVs.

The basic configuration was used on a total of 5 designs, the P208 through P215 [1]. Several of these designs are shown in Figure 2. The most mature design was for the P208/03, shown in Figure 3, with considerable documentation found at the wars end. Prototypes of the P208/03 where ordered, but the war ended before any work could begin and none were ever built [2].

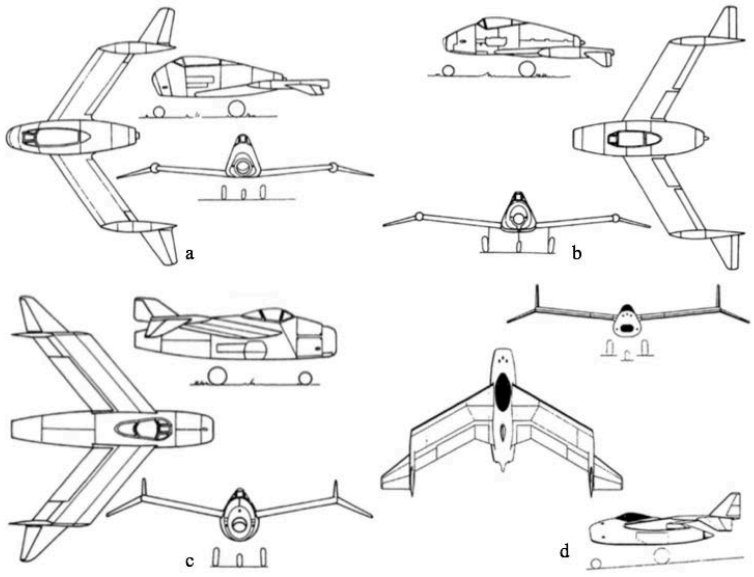

Figure 2. Several Blohm & Voss Semi-Tailless Designs [4].

Figure 3. Blohm & Voss P208/03 [2].

More recently the configuration has been evaluated to determine whether it is viable, and if the assumed benefits exist. Tipton [5] performed a preliminary design exercise to predict P208/03's performance and stability and control. By using empirical data on wing tip vortex formation, the flow field impacting the stabilizer was predicted. It was shown that unless the aircraft was at a large angle of attack or had a large flap deflection there was no significant increase

in the angle of attack or the velocity from free stream conditions seen by the stabilizer. However, the angle of attack and velocity was greater than would be seen if the stabilizer was behind the wing. A component-build-up method was used to predict the aircraft drag, and it was shown that the parasite drag was as much as 25% lower than similar designs of the time. It was also shown that the aircraft was stable and trimmable in all flight conditions and had reasonable handling qualities.

Muller [6] further investigated the P208/03's performance, stability, and control using more sophisticated methods. The aircraft's static stability and performance was analyzed using a vortex lattice solver. The results from this work indicate the aircraft is stable and trimmable in all flight conditions, although with flaps deflected large elevator deflections of 20 degrees or more were required for trim. The dynamic stability was also analyzed in greater detail, with more negative results. Although it had good handling qualities in longitudinal modes, the lateral-directional modes, specifically dutch-roll, had deficiencies. Other than in a cruise condition the aircraft was unstable in dutch-roll. Although a yaw-damper would likely correct the issue, more investigation is required to confirm.

There are also lingering structural concerns that have not been investigated. The stabilizers location aft of the wing tips will likely generate large torsional loads in the wing. If these torsional loads require significant reinforcement then the reduction in weight will be offset, reducing the concept's benefits. This concern may be reduced on small UAVs due to structural scaling effects.

While not widely applied, aircraft with similar configurations have been investigated. Extensive investigations have been made by John Kentfield [4] from the University of Calgary on an OHS concept. The designs share a few characteristics but are notably different due to mission goals. Where the designers at Blohm & Voss sought to minimize weight and wetted area to

maximize speed, Kentfield has focused on maximizing the lift-to-drag ratio. The designs feature straight wings, with the stabilizer mounted two to four chord lengths aft of the trailing edge. The stabilizer area is also not reduced as leaving them larger increases the total aircraft lift-to-drag. An aircraft using the OHS configuration designed for an SAE Aero Design competition, is shown in Figure 4.

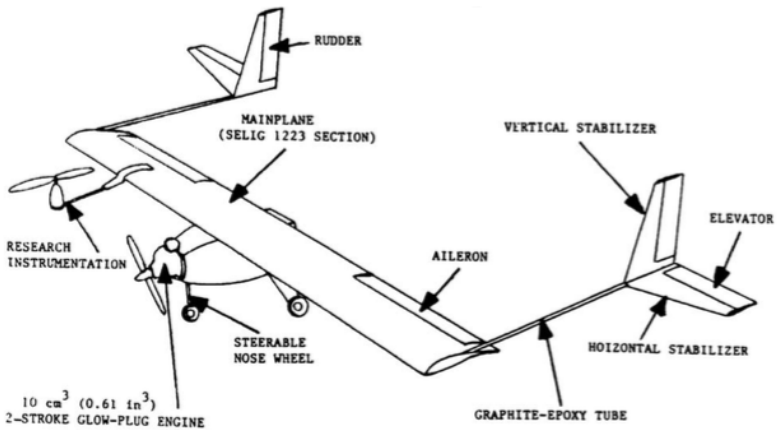

Figure 4. Outboard Horizontal Stabilizer SAE Aero Design Contest Aircraft [4].

1.3 Variable Cant Angle Stabilizers

On the original B&V concept, the stabilizers were mounted at a fixed cant angle (shown in Figure 5) and featured trailing edge control surfaces which acted as ruddervators. Many factors went into the final selection of size and cant angle for the stabilizers but providing adequate longitudinal and lateral-directional stability were likely the key requirements, with performance being a secondary concern. However, no investigations have been done to determine what affect changing the stabilizer cant angle has on aircraft performance, and the selected cant angle may not be optimal for all flight phases. If a large impact on performance is found across different flight phases, then it may be desirable to change the cant angle in flight to improve performance.

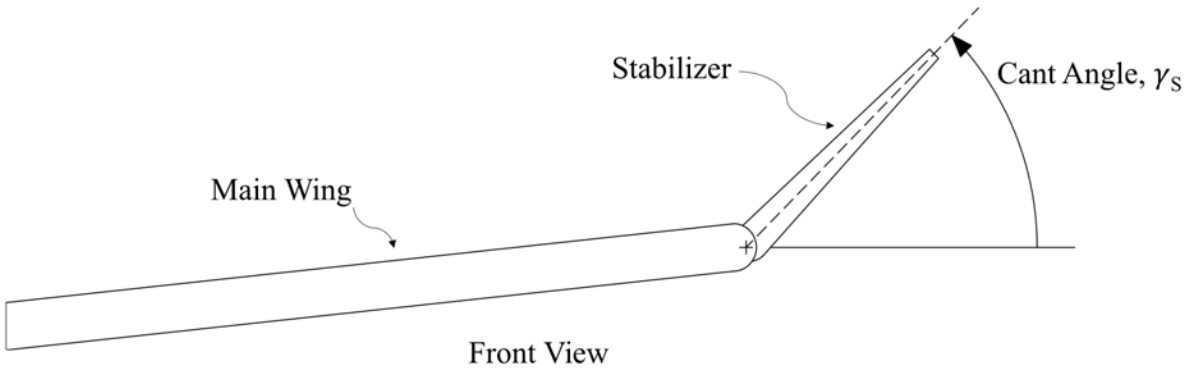

Figure 5. Definition of stabilizer cant angle.

While it may be possible to improve performance, changing the cant angle in flight will also have a dramatic impact on the stability and control, both longitudinally and lateral-directionally. This could create issues, but it may also be possible to harness these effects to also provide control. If the cant angle that provides the optimal performance characteristics for a given flight phase also naturally trims the aircraft for that phase, then the action of trimming the aircraft will put it into the optimal configuration for the flight phase.

Bourdin, Gatto, And Friswell [7][8][9][10] have conducted analysis and wind tunnel testing on a flying wing design with variable cant winglets, demonstrating it is a valid method of control. A commercially available flying wing was modified so that the outboard wing could be deflected, as show in Figure 6. The studies have shown that the wingtips can be used to successfully control aircraft roll and yaw, as well as pitch. While proverse yaw was found to be possible, the yawing moment was smaller than desired. The control in pitch was also found to be less than desired. On the B&V concept the stabilizer is aft of the trailing edge and will create larger pitching and yawing moments, likely providing more control.

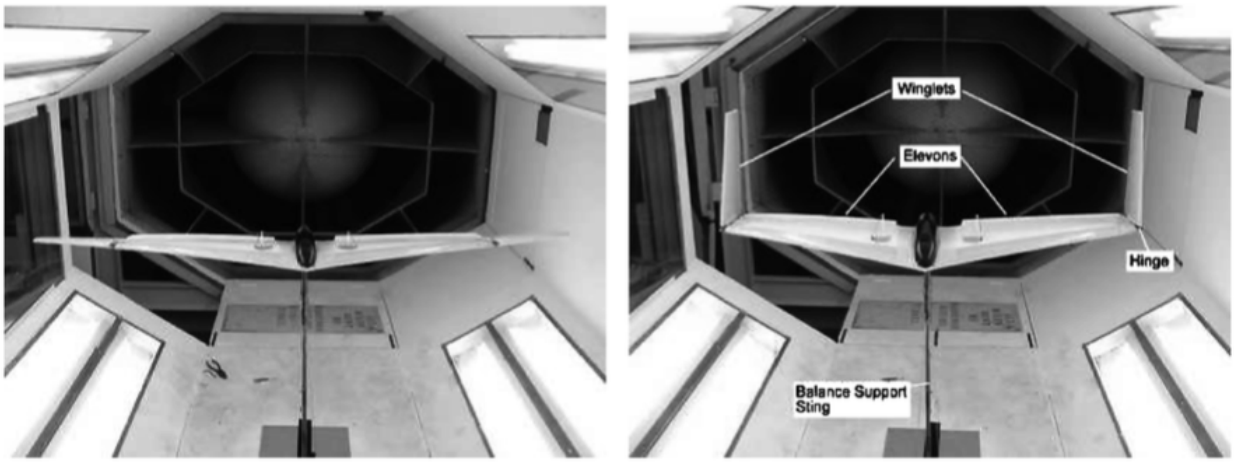

Figure 6. Bourdin flying wing in wind tunnel [8].

1.4 Objective

The main objective of this thesis was to determine if the B&V semi-tailless concept is a viable concept for small UAVs, and if utilizing variable cant-angle stabilizers is a viable control concept. The B&V P208/03 geometry is scaled down and is used to establish a baseline configuration. A simple analytical model was developed to allow the variable cant configuration to be quickly analyzed and trade studies done to determine which parameters have the largest impact and establish a narrower design space. Then vortex lattice solvers were used to further analyze the design, providing more detailed results and performance predictions.

A wind tunnel and flight test model was constructed to validate the results. The model was wind tunnel tested in the WSU 3x4 Low Speed Wind Tunnel to validate the longitudinal stability and performance predictions. Finally, the model was flight tested to provide qualitative pilot feedback and handling quality ratings.

CHAPTER 2

METHODS

2.1 Simple Analytical Model

2.1.1 Assumptions and Limitations

The main goal of this simple analytical model is to predict the basic aircraft stability and control, and assumptions are made to simplify the model without limiting this ability. In a conventional aircraft the downwash and reduction in velocity behind the wing must be considered. However, in the B&V semi-tailless configuration the stabilizers are in a region of upwash and no velocity deficit and this should be considered. Tipton [5] analyzed the flow field around the stabilizer and found that unless the wing was at a large angle of attack or there were large flap deflections, there was a negligible effect on stabilizer flow field, so this affect is not included in the simple analytical model. This model does not predict the aircraft drag, as the drag will depend on the complex interaction of wing tip vortices with the stabilizer and will be very difficult to model. The model is also developed using only symmetric airfoils but can be easily modified to included cambered airfoils.

2.1.2 Stabilizer Aerodynamic Forces

Before developing equations to calculate forces and moments on the entire aircraft, the force generated by only the stabilizers are first analyzed. The total stabilizer aerodynamic force is given by

$$F_S = C_{L_{\alpha_S}} \alpha_S S_S q_\infty \tag{1}$$

where α_S is the local angle of attack seen by the stabilizer, which is assumed constant over the stabilizer span. The local angle of attack seen by the stabilizer is a function of cant angle, γ_S,

incidence angle, i_S, toe angle, t_S, aircraft angle of attack, α, and aircraft sideslip, β. In general, the local angle of attack is given by equation (2).

$$\alpha_S = (\alpha + i_S)\cos\gamma_S + (\beta + t_S)\sin\gamma_S \quad (2)$$

The incidence and toe angles describe the stabilizer axis of rotation orientation relative to the wing tip, as shown in Figure 7. These angles may allow for additional control over aircraft stability and control.

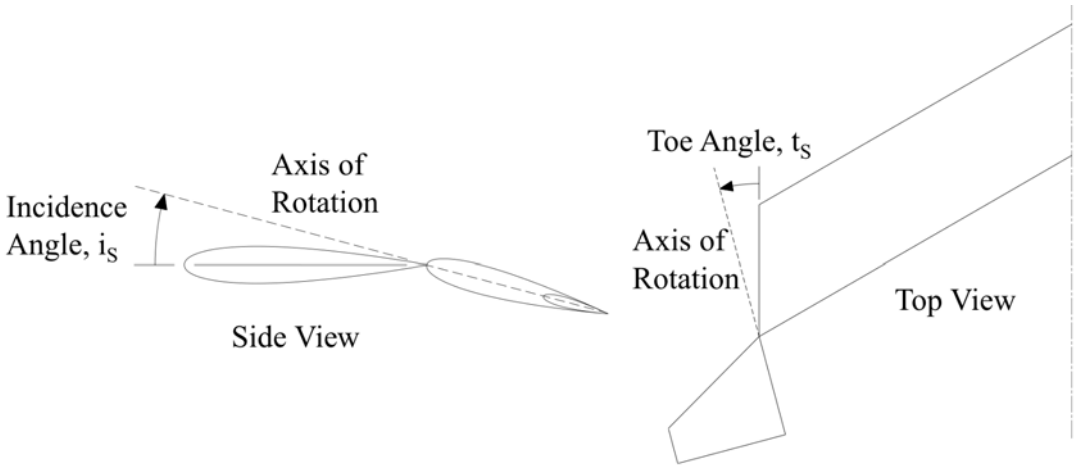

Figure 7. Definitions of toe and incidence angles.

The toe angle is defined relative to the wing tip, so local of angle of attack may not be the same for the left and right stabilizers, as shown in Figure 8. As can be seen the sideslip increases the local angle of attack seen by the left stabilizer but reduces local angle of attack seen by the right stabilizer. This leads to the equations for the local of attack given by equation (3) and (4).

$$\alpha_{S_L} = (\alpha + i_S)\cos\gamma_{S_L} + (t_S + \beta)\sin\gamma_{S_L} \quad (3)$$

$$\alpha_{S_R} = (\alpha + i_S)\cos\gamma_{S_R} + (t_S - \beta)\sin\gamma_{S_R} \quad (4)$$

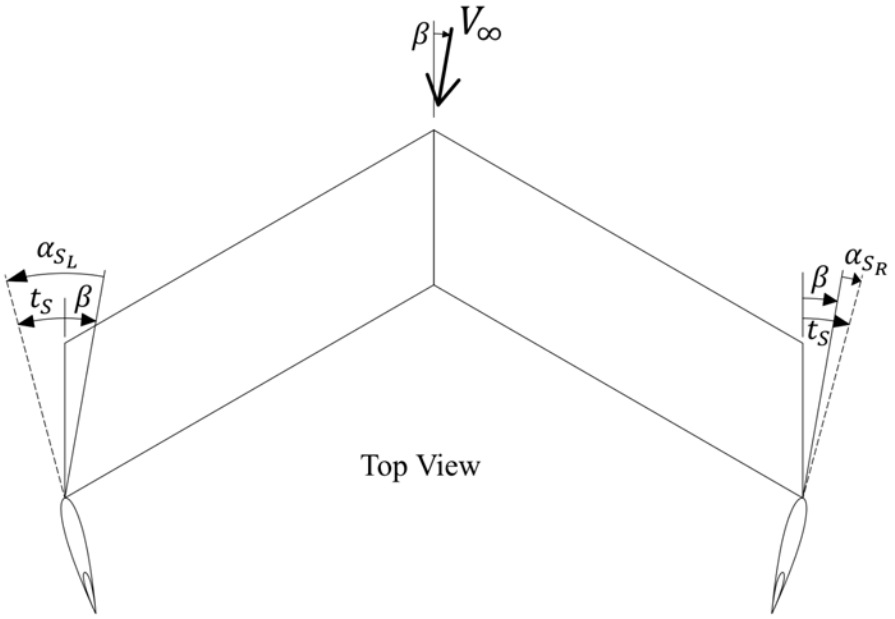

Figure 8. Local angle of attack seen by stabilizers at 90° cant angle with sideslip.

Once the local angle of attack is known, then the total force generated by the stabilizers can be found by substituting equations (3) or (4) into equation (1). The force generated by the stabilizer will be normal to the surface, and its direction can be found using the cant angle. For calculating forces and moments on the entire aircraft it will be more useful to know the components in the y and z directions, L_S and Y_S, as shown in Figure 9, which leads to equation (5) and (6). If the stabilizer is mounted with a toe angle than there will also be a component of the force acting in the x-direction, however, if the toe angle is small this force will be small and can be neglected.

$$L_S = F_S \cos \gamma_S \tag{5}$$

$$Y_S = F_S \sin \gamma_S \tag{6}$$

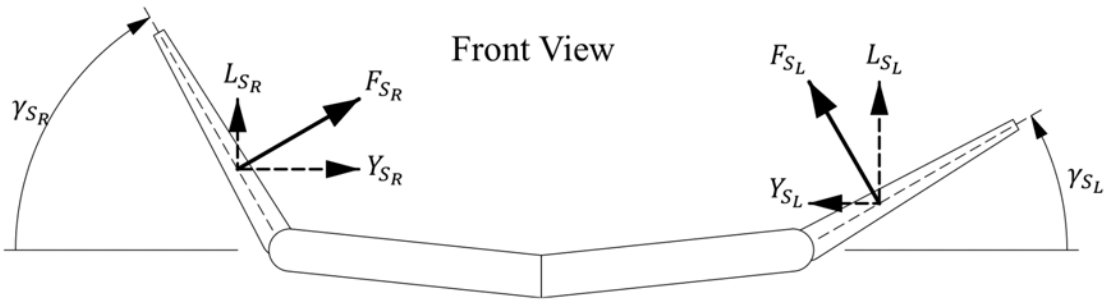

Figure 9. Components of total stabilizer force in x and y directions.

2.1.3 Aircraft Lift

Once the forces generated by the stabilizers is known then total aircraft forces and moments can be found. The forces and moments acting in the Z-direction are shown in Figure 10. It can be seen that the only contribution to lift is from the wing and stabilizers, given by equation (7).

$$L = L_W + L_{S_R} + L_{S_L} \tag{7}$$

The main wing will feature flaps, so this needs to be included in the lift calculated by the wing. One way to represent the flaps is as a change in the angle of zero lift. Raymer [11] gives the change in angle of zero lift per flap deflection as

$$\frac{\Delta\alpha_{0_L}}{\delta_f} = \left(-\frac{1}{C_{L_\alpha}}\frac{\partial C_L}{\partial \delta_f}\right) \tag{8}$$

where

$$\frac{\partial C_L}{\partial \delta_f} = 0.9K_f\left(\frac{\partial C_l}{\partial \delta_f}\right)_{airfoil}\frac{S_{flapped}}{S_w}\cos\Lambda_{H.L.} \tag{9}$$

the terms K_f and $\frac{\partial C_l}{\partial \delta_f}$ can be estimated using Figure 16.6 and Figure 16.7 in reference [11]. Non-dimensionalizing equation (7) and substituting equations (1), (5), and (8) result in equation (10).

$$C_L = C_{L_{0_w}} + C_{L_{\alpha_w}}\left(\alpha + \frac{\Delta\alpha_{0_L}}{\delta_f}\delta_f\right) + C_{L_{\alpha_S}}\frac{S_S}{S_W}\left[\alpha_{S_R}\cos\gamma_{S_R} + \alpha_{S_L}\cos\gamma_{S_L}\right] \tag{10}$$

Note that if the stabilizers are rotated symmetrically and there is no sideslip the two terms for the stabilizers can be combined into a single term, but two terms are necessary if they are rotated asymmetrically for roll/yaw control.

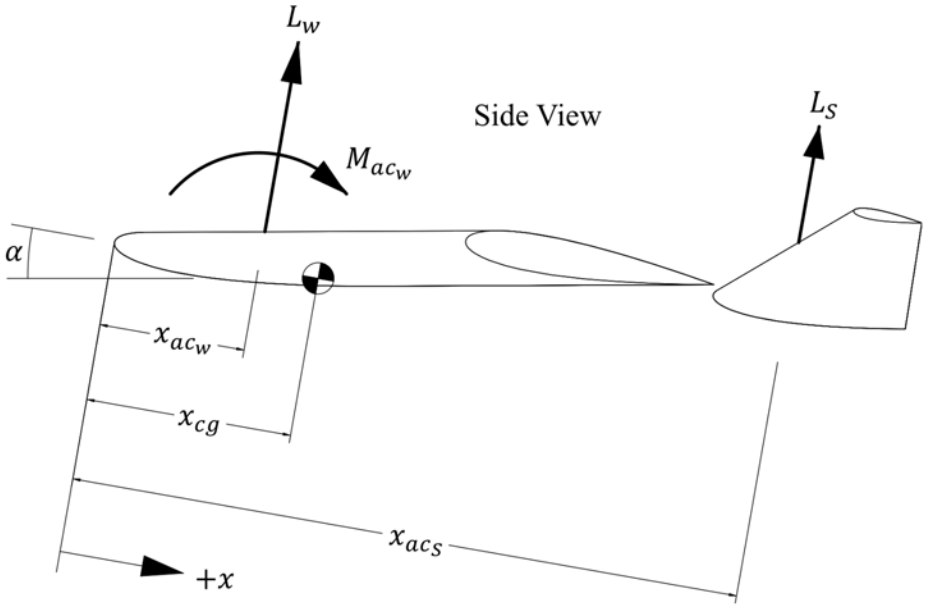

Figure 10. Forces and moments for calculating lift and pitching moment.

2.1.4 Aircraft Pitching Moment

Referring back to Figure 10, there are three forces and moments that need to be considered for the pitching moment, given by equation (11).

$$M = M_{ac_w} + M_{\delta_f} + L_w\left(x_{cg} - x_{ac_w}\right)\cos\alpha - L_{S_R}\left(x_{ac_S} - x_{cg}\right)\cos\alpha - L_{S_L}\left(x_{ac_S} - x_{cg}\right)\cos\alpha \tag{11}$$

The effect of flaps must also be included in the aircraft total pitching moment. From Raymer [11] the pitching moment due to flaps is given by

$$C_{M_{w\delta_f}} = -\frac{\partial C_L}{\partial \delta_f}\left(\bar{x}_{cp} - \bar{x}_{cg}\right) \tag{12}$$

where $\bar{x}_{cp}$ can be estimated using Figure 16.9 in reference [11].

As the stabilizers rotate x_{ac_S} does not change and is the same for both stabilizers. Using small angles, $\cos\alpha \approx 1.0$, non-dimensionalizing, and substituting for L_{S_R} and L_{S_L} results in equation (13).

$$C_M = \left[C_{L_{0_w}} + C_{L_{\alpha_w}}\left(\alpha + \frac{\Delta\alpha_{0_L}}{\delta_f}\delta_f\right)\right](\bar{x}_{cg} - \bar{x}_{ac_w}) - C_{M_{w\delta_f}}\delta_f -$$

$$C_{L_{\alpha_S}}(\alpha_{S_R}\cos\gamma_{S_R} + \alpha_{S_L}\cos\gamma_{S_L})(\bar{x}_{ac_S} - \bar{x}_{cg})\frac{S_S}{S_w} \quad (13)$$

2.1.5 Aircraft Rolling Moment

The models primary concern is to predict the stabilizers effect on the aircraft, and as such the wings effect on rolling moment will not be analyzed in detail. The diagram in Figure 11 shows the forces and distances needed to calculate rolling moment.

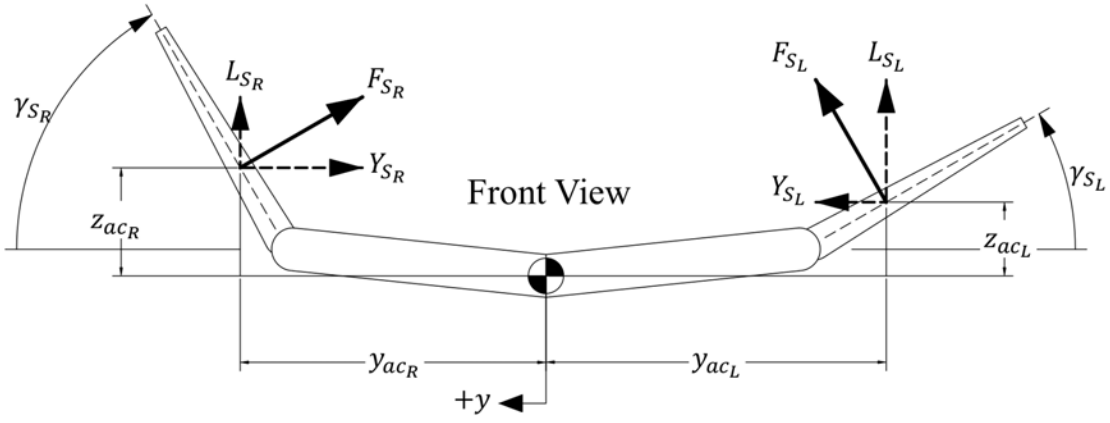

Figure 11. Forces for calculating rolling moment and sideforce.

The rolling moment about the CG location is given by equation (14), shown below.

$$L_A = L_W - L_{S_L}y_{ac_L} - L_{S_R}y_{ac_R} + Y_{S_L}z_{ac_L} - Y_{S_R}z_{ac_R} \quad (14)$$

Non-dimensionalizing the equation and substituting equations (5) and (6) lead to equation (15).

$$C_l = C_{l_{\beta_W}}\beta + C_{L_{\alpha_S}}\frac{S_S}{S_W}[-\alpha_{S_R}\bar{y}_{ac_R}\cos\gamma_{S_R} - \alpha_{S_L}\bar{y}_{ac_L}\cos\gamma_{S_L} +$$

$$\alpha_{S_R}\bar{z}_{ac_R}\sin\gamma_{S_R} - \alpha_{S_L}\bar{z}_{ac_L}\sin\gamma_{S_L}] \quad (15)$$

Unlike x_{ac_S} the reference distances for rolling moment may not be the same for both stabilizers, and the distances will also depend on the stabilizers' cant angle. These relationships are given by equation (16) and (17).

$$y_{ac_S} = y_{AR} + \bar{Y}_S \cos\gamma_S \tag{16}$$

$$z_{ac_S} = z_{AR} + \bar{Y}_S \sin\gamma_S \tag{17}$$

where y_{AR} is spanwise distance from the CG to the axis of rotation, z_{AR} is the vertical distance from the CG to the axis of rotation, and $\bar{Y}_S$ is the stabilizer MAC spanwise location.

2.1.6 Aircraft Side-Force

Referring back to Figure 11, it can be seen that the side-force of the entire aircraft is given by equation (18).

$$Y_A = Y_{A_w} + Y_{S_L} - Y_{S_R} \tag{18}$$

Non-dimensionalizing the equation results in equation (19).

$$C_Y = C_{Y_{\beta_w}}\beta + C_{L_{\alpha_S}}\frac{S_S}{S_W}\left[\alpha_{S_L}\sin\gamma_{S_L} - \alpha_{S_R}\sin\gamma_{S_R}\right] \tag{19}$$

2.1.7 Aircraft Yawing Moment

The forces that impact the yawing moment are shown in Figure 12. The main driver of the yawing moment is the side-force generated by the stabilizers. The yawing moment equation is given in equation (20).

$$N_A = N_{A_W} + Y_{S_R}\left(x_{ac_S} - x_{cg}\right) - Y_{S_L}\left(x_{ac_S} - x_{cg}\right) \tag{20}$$

Non-dimensionalizing the equation results in equation (21).

$$C_n = C_{n_{\beta_w}}\beta + C_{L_{\alpha_S}}\left(\alpha_{S_R}\sin\gamma_{S_R} - \alpha_{S_L}\sin\gamma_{S_L}\right)\left(x_{ac_S} - x_{cg}\right)\frac{S_S}{S_W} \tag{21}$$

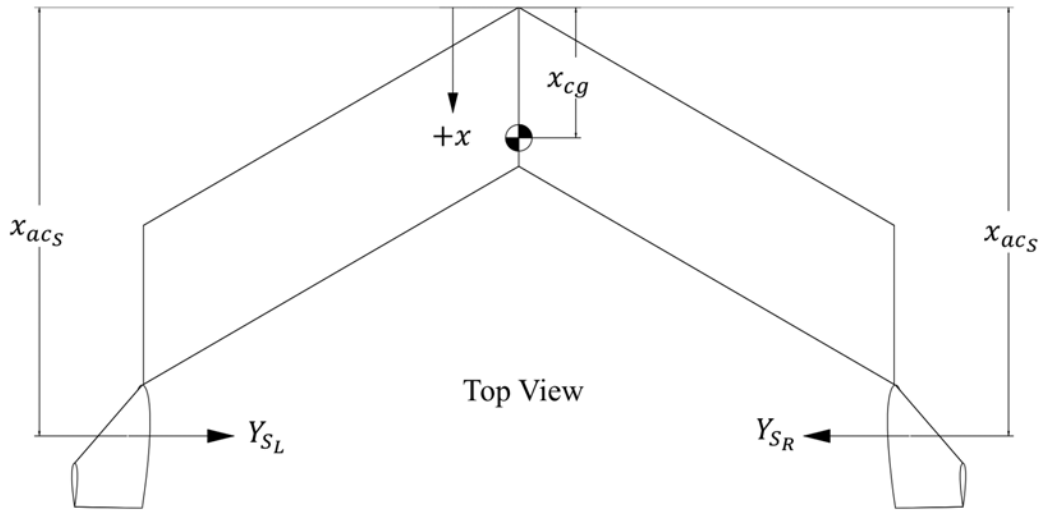

Figure 12. Forces for calculating yawing moment.

2.1.8 Discussion

It can be seen that the local angle of attack for the stabilizers occurs in every equation. The local angle of attack is a function of both angle of attack and sideslip and means that sideslip will impact the aircraft's longitudinal behavior, and the sideslip will impact the lateral-directional behavior. This prevents the equations of motion from being broken into distinct longitudinal and lateral-directional equations. If solving for the trim conditions all five non-linear equations must be solved simultaneously. Obviously, this should not be a difficult challenge with a computer program.

A key parameter of longitudinal stability, C_{M_α}, can be found by differentiating equation (13) with respect to angle of attack to arrive at equation (22), shown below.

$$\frac{\partial C_M}{\partial \alpha} = C_{L_\alpha}\left(\bar{x}_{cg} - \bar{x}_{ac_w}\right) + \left(\cos^2 \gamma_{S_R} + \cos^2 \gamma_{S_L}\right)\left(\bar{x}_{ac_S} - \bar{x}_{cg}\right) C_{L_{\alpha_S}} \frac{S_S}{S_w} \tag{22}$$

This term must be less than zero to ensure static stability in pitch. This is usually accomplished by ensuring that the CG location is ahead of the neutral point. Examining equation (22) it can be seen that the stabilizers' cant angle shows up in the equation. This means that changing cant angle will

change the aircraft's pitch stability, as shown in Figure 13. This affect can be harnessed to trim the aircraft, but the CG location must be carefully chosen so that the aircraft will be stable for all possible cant angles. Additionally, deflecting only one stabilizer at a time to control roll/yaw will also create changes in the pitch stability and trim.

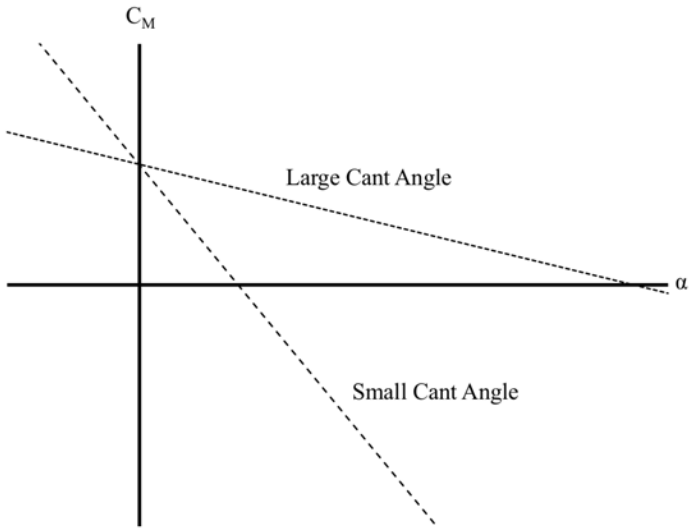

Figure 13. Effect of cant angle on C_{M_α}.

2.2 Potential Flow Methods

Vehicle Sketch Pad, or OpenVSP [12] is an open source parametric aircraft design tool developed by NASA [13]. The program allows users to quickly generate aircraft geometries for conceptual and preliminary designs. Included in the package is an aerodynamic analysis tool, VSPAERO. This tool uses potential flow solvers to analyze the aerodynamics and stability and control of a design. Two solvers are included, a vortex lattice solver and a panel method solver. A main concern of the design is the wing tip vortex impact, which is not included in the simple analytical model, and the vortex lattice solver is well suited to modeling this behavior and is used exclusive for this thesis. OpenVSP also has a python API which allows the user to change design

geometry programmatically. Scripts can also be created to automate VSPAERO. Both of these features make it useful for doing large batches of runs when doing trade studies.

OpenVSP can accurately predict the aircraft induced drag, but because it is a vortex lattice solver it cannot predict parasite drag. While additional features have been added to predict the parasite drag, these tools assume a much larger Reynolds number than what will be expected for small UAVs. A separate method given by Nicolai [14] is used to predict parasite drag. This method is specifically suited for small, low-Reynolds number UAVs, and provides good estimates of drag at these conditions.

2.3 Validation

Bourdin et. al. [7], [8] investigated the use of variable cant angle winglets on a flying wing for control. They utilized a vortex lattice solver to make predictions of aircraft forces and moments. Unlike the B&V concept whose stabilizers are aft of the wing tip, the flying wing model used winglets mounted directly to the wing tip. The flying wing also utilized a cambered airfoil sections, this camber will be accounted for by adding a $C_{L_{0_S}}$ term in the equations for stabilizer lift. The pitching moment created by the cambered section was not included in the model. An OpenVSP model was also generated, as shown in Figure 14.

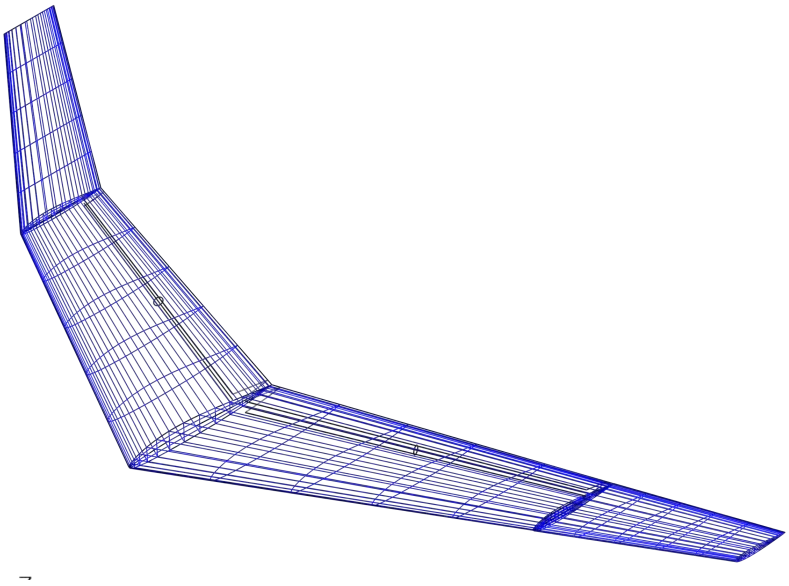

Figure 14. OpenVSP model of Bourdin [7] flying wing.

After making predictions using a vortex lattice solver, Bourdin et.al. then wind tunnel tested a model. The model was examined at a fixed angle of attack and the right winglet cant angle was varied from -90° to +90°. The angle of attack was selected so that the aircraft has a C_L of 0.4 with both winglets at a cant angle of 0° (flat). The model was tested in a closed test section wind tunnel, shown in Figure 6, at a Reynolds number of 230,000. The results of testing are shown in Figure 15.

While all of the methods provide similar predictions, there are some differences between the predictions and the wind tunnel results. The pitching moment has the largest difference, but Bourdin et. al. attribute this to large aeroelastic effects seen on the elevator of the wind tunnel model. Results for the wing at a C_L of 0.2 was also presented, and shows similar differences but at half the magnitude, implying that the aeroelastic effects are the likely cause. There are also differences seen in the yawing moment, but this could also be due to aeroelastic effects, or low-Reynolds number effects. Despite these differences, there is confidence that the simple analytical model and OpenVSP can provide accurate predictions.

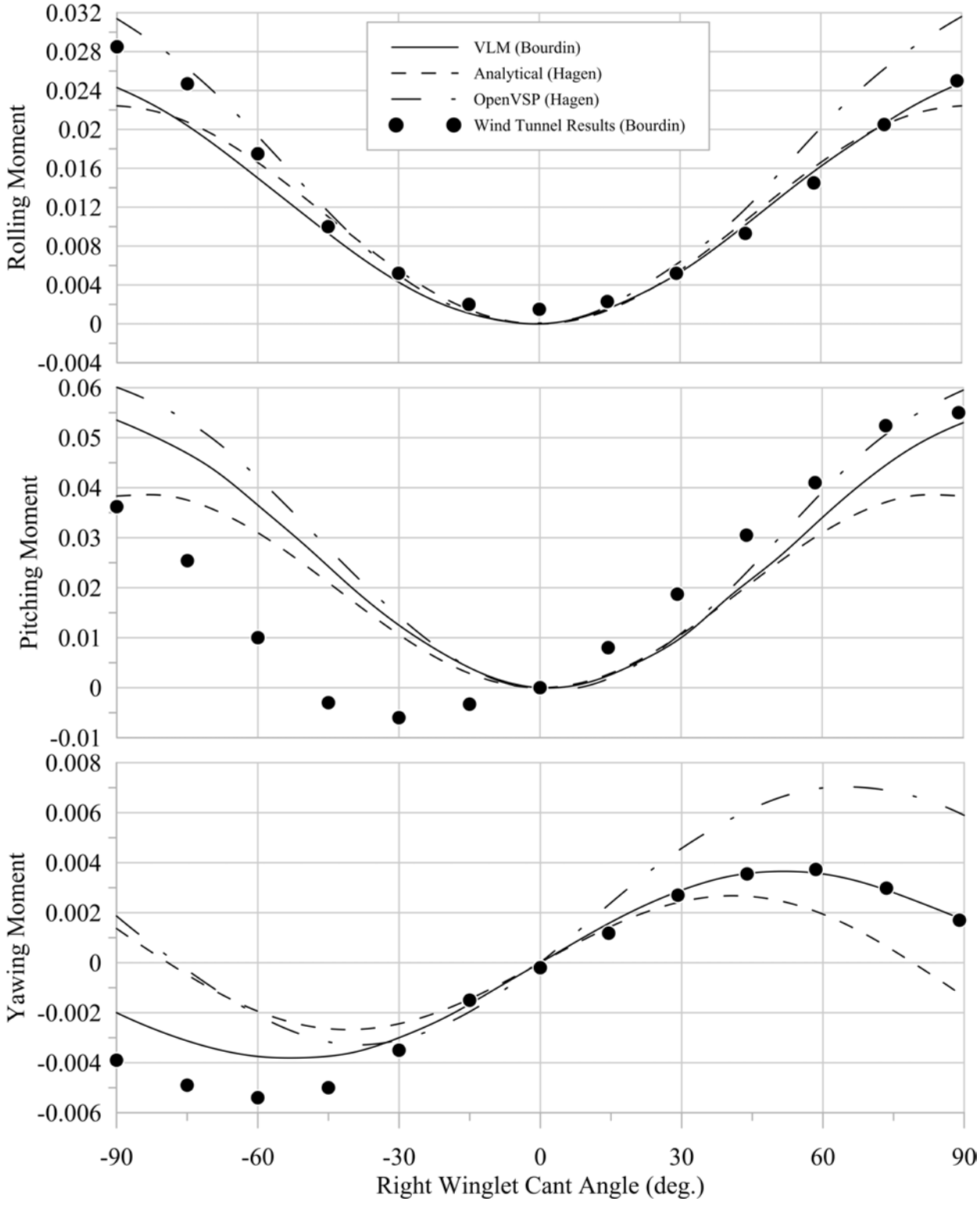

Figure 15. Rolling, pitching, and yawing moments for Bourdin [7] flying wing.

CHAPTER 3

BASELINE CONFIGURATION

3.1 Geometry

Before considering the variable cant stabilizers a baseline configuration was first evaluated. The B&V P208/03, the focus of previous research, was selected as the baseline. A three-view drawing is shown in Figure 16, and some basic geometric data is given in Table 1. This baseline was then analyzed to determine its viability for small UAVs and to identify if any design changes are required. The baseline was then used to compare the variable cant configuration performance.

Due to time constraints only a single model is constructed and some modifications made to ensure it would work for all anticipated configurations and to simplify analysis and construction. The following changes to the geometry were made: fillets at the wing root were removed, the wing and stabilizer incidence angle was set to zero, and the fuselage was ignored for the majority of the analysis.

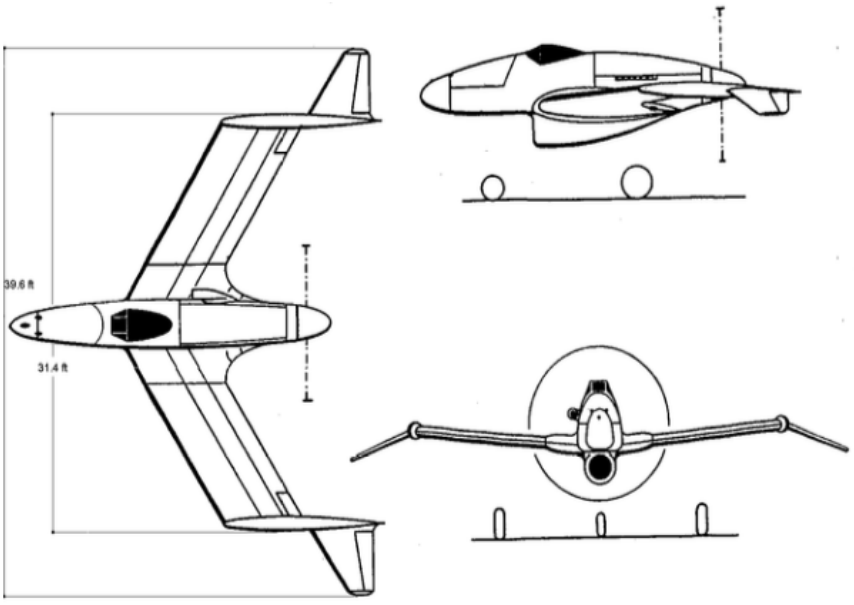

Figure 16. Blohm & Voss P208/03 three-view drawing [2].

TABLE 1

GEOMETRIC INFORMATION FOR BLOHM & VOSS P208/03 [6]

Parameter	**Value**	
Total Span (ft)	39.62	
Total Length (ft)	30.18	
Total Height (ft)	11.35	
	Wing	**Stabilizer**
Span (ft)	31.42	11.15
Root Chord (ft)	6.56	5.08
Tip Chord (ft)	6.56	1.80
Aspect Ratio	4.75	3.24
Taper Ratio	1.00	0.36
1/4 Chord Sweep Angle	30.0°	24.7°
Dihedral/Cant	6.0°	-20.0°
Incidence	2.0°	-3.5°

In reference [3] the airfoil is given as “BVH 12%.” This is a 12% thick airfoil designed by B&V, however the specific profile is not available. Tipton [5] and Muller [6] both used a NACA 23012 in their analysis as it was representative of airfoils available at the time and had good performance. While this airfoil should work, the pitching moment characteristics required for the multiple configurations was not known when beginning analysis. This led to the selection of a NACA 0015 for both the main wing and the stabilizers. The NACA 0015 has robust performance at low-Reynolds numbers, is fairly tolerant to construction errors, and the symmetric cross section makes it easier to modify the pitching moment to the desired characteristics using trailing edge flaps. OpenVSP also defines the airfoil parallel to the aircraft centerline, and not perpendicular to the wing leading edge, so this is how the airfoil is defined for the aircraft.

The main wing will feature 25% chord plain flaps which spanned the outboard 50% of the wing. These flaps can be used as elevons or flaperons, depending on the configuration requirement. They are also be used to adjust the wing pitching moment characteristics depending on configuration requirements. The baseline aircraft also features elevators on the stabilizers. They are 30% chord plain flaps which extend over the entire span.

3.2 Sizing

Only a single model was constructed and is used for both flight and wind tunnel testing, and these two purposes were considered when sizing the aircraft. A hand-launch, and later bungee-launch, was the selected takeoff method. This provided the most flexibility in CG location, and also the lowest aircraft weight. To improve the chance of a successful launch the aircraft was made with as low a stall speed as possible. The WSU 3'x4' Low Speed Wind Tunnel (LSWT) was used to test the model. This tunnel has a width of 4.2 feet. Pope, et. al. [15] recommends that the model span not exceed 80% of the tunnel width. The aircraft was made as large as possible, while not exceeding this limit, which resulted in the lowest stall speed. The final scaled geometry is shown in Table 2.

TABLE 2

GEOMETRIC DATA FOR BASELINE CONFIGURATION

Parameter	**Wing**	**Stabilizer**
Span (ft)	2.40	0.85
Root Chord (ft)	0.50	0.39
Tip Chord (ft)	0.50	0.14
Aspect Ratio	4.75	3.24
Taper Ratio	1.00	0.36
1/4 Chord Sweep Angle	30.0°	24.7°
Dihedral/Cant	6.0°	-20.0°
Incidence	0.0°	-3.5°

3.3 Results

The geometry was modeled in OpenVSP, as shown in Figure 17. The OpenVSP model used 24 spanwise panels and 16 chordwise panels on the main wing, and 6 spanwise panels and 16 chordwise panels on each stabilizer. Increasing the number of panels was not found to improve results.

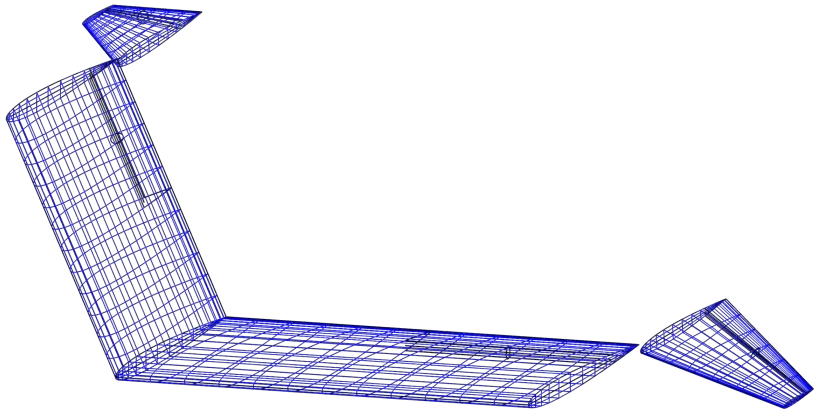

Figure 17. OpenVSP model of Baseline configuration.

OpenVSP cannot predict stall, so a method given by Raymer [16] was used to predict $C_{L_{max}}$. The NACA 0015 has a $c_{l_{max}}$ of 1.0 at a Reynolds number of 331,00 [17], which leads to an aircraft $C_{L_{max}}$ of 0.8. The OpenVSP results are limited to angles of attack where C_L is below this value.

3.3.1 Longitudinal Stability and Control

Ensuring that the aircraft is stable and trimmable longitudinally is the critical requirement for a viable aircraft. To ensure the aircraft is stable the CG location was set at 31.5% MAC, which provided a static margin of 16%. The longitudinal stability derivatives for the baseline in cruise are shown in Table 3, which show the aircraft is stable. Multiple elevator deflections were checked to ensure that the aircraft can trim across the entire C_L range. The trim plot, Figure 18, shows that

the aircraft can trim at $C_{L_{max}}$ (0.8) with an elevator deflection of -15° which allows sufficient control margin.

TABLE 3

LONGITUDINAL STABILITY DERIVATIVES IN CRUISE

Stability Derivatives (per Radian)					
C_{L_α}	4.3	C_{L_q}	4.46	$C_{L_{\delta_e}}$	0.31
C_{D_α}	0.15	C_{D_q}	0.26	$C_{D_{\delta_e}}$	0.02
C_{M_α}	-0.76	C_{M_q}	-4.45	$C_{M_{\delta_e}}$	-0.58

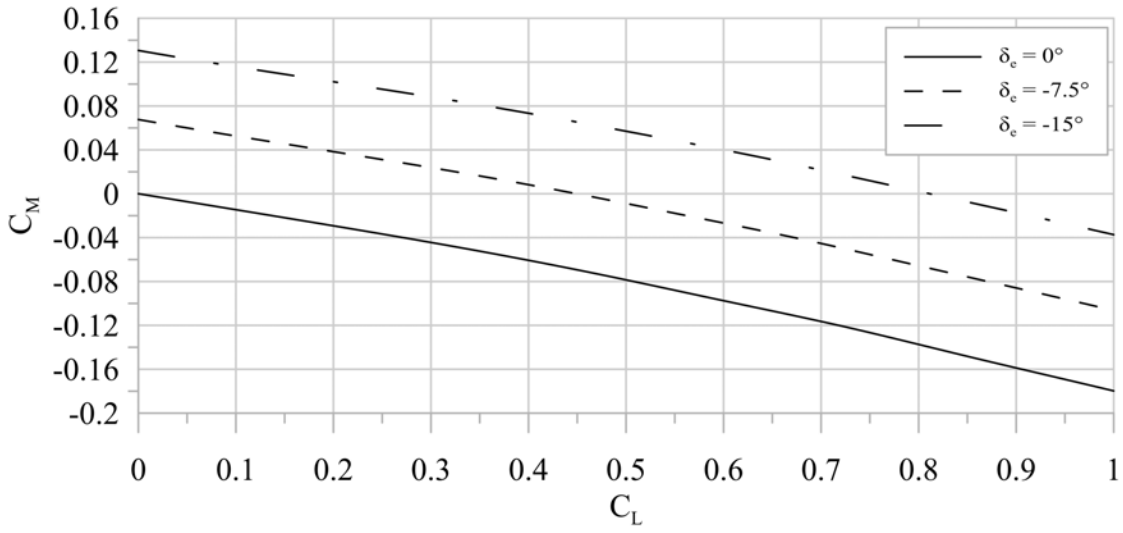

Figure 18. Trim plot for baseline configuration from OpenVSP.

3.3.2 Lateral-Directional Stability and Control

Ensuring that the aircraft is stable lateral-directionally is also a key requirement for a viable aircraft. Looking at the P208/03 it appears to have small vertical stabilizers. The only vertical surface on the aircraft is the area projected onto the vertical plane by the stabilizers. Raymer [18] recommends tail volume coefficients of 0.04-0.07, but the P208/03 only has a vertical tail volume

coefficient of 0.024. Table 4 shows the lateral-directional stability derivatives which show that the aircraft is statically stable, but the yaw stability is marginal. Additional vertical surfaces will be added for initial test flights and will then be removed for later test flights. Many other B&V designs featured vertical fins mounted next to the stabilizers, as shown in Figure 2, but the precise vertical tail form will be determined after analysis of the variable cant configuration.

TABLE 4

LATERAL-DIRECTIONAL STABILITY DERIVATIVES IN CRUISE

Stability Derivatives (per Radian)							
C_{Y_β}	-0.07	C_{Y_p}	0.26	C_{Y_r}	0.04	$C_{Y_{\delta_r}}$	-0.5
C_{l_β}	-0.07	C_{l_p}	-0.73	C_{l_r}	0.05	$C_{l_{\delta_r}}$	0.30
C_{n_β}	0.02	C_{n_p}	-0.20	C_{n_r}	-0.02	$C_{n_{\delta_r}}$	0.02

Another interesting property of the typical B&V design is that the ailerons create proverse yaw. In the baseline configuration the main wing control surfaces are used as ailerons, and these will have a large impact on the wing tip vortex. Deflecting the ailerons down increases the wing tip vortex strength, which increases the stabilizer lift. This lift acts outwards, which creates a positive yawing moment. If the stabilizers where mounted with a positive cant angle instead of a negative cant angle this benefit would not occur, and severe adverse yaw would be generated.

3.3.3 Drag

The method of Nicolai [14] was used to predict the aircraft C_{D_0}. To get a better estimate a sample fuselage was generated but does not represent the final fuselage selection. The aircraft with a fuselage and wing tip pods is shown in Figure 19. A cruise speed of 60 ft/s was chosen, which results in a Reynolds number of 200,000 based on the wing chord. The predicted C_{D_0} is 0.0232,

and when combined with OpenVSP's prediction of induced drag a complete drag polar is generated, shown in Figure 20.

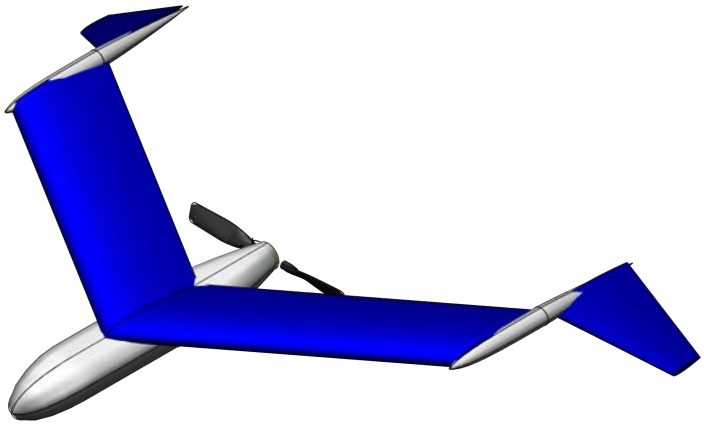

Figure 19. Baseline configuration with simple fuselage.

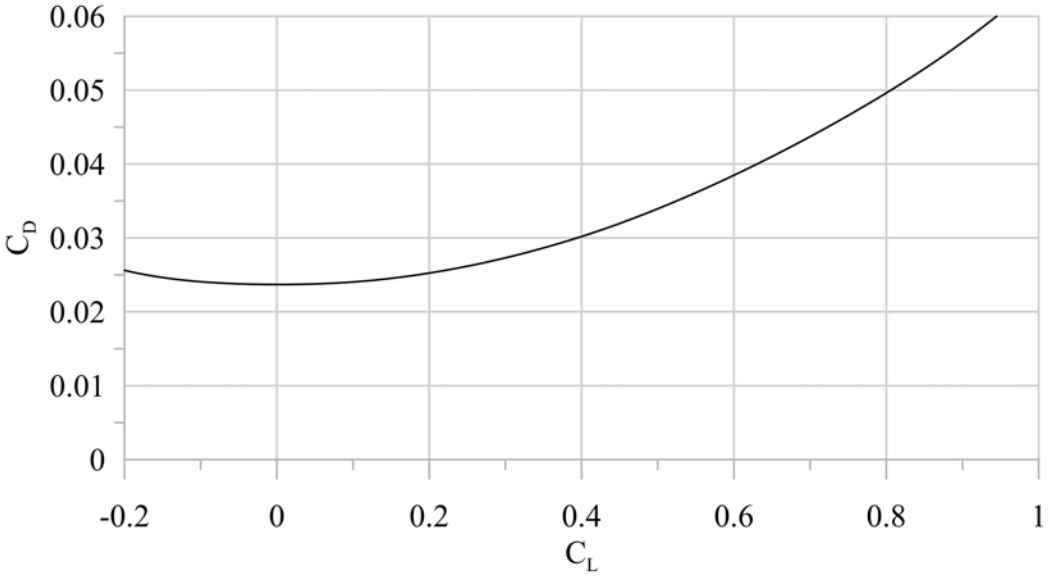

Figure 20. Drag polar for baseline configuration from OpenVSP.

CHAPTER 4

VARIABLE CANT CONFIGURATION

4.1 Introduction

This chapter will discuss using the variable cant stabilizers for aircraft control. Three main modes are considered: longitudinal control, lateral-directional control, and combined control where the stabilizer are used to control both longitudinal and lateral-directional forces and moments simultaneously. For longitudinal control the stabilizers will both have the same cant angle and will be varied to affect trim. Lateral-directional control will be achieved by changing the cant angle of one stabilizer, while the other remains fixed. In the results presented the left stabilizer remains fixed and the right stabilizer cant angle is changed. These can be reversed to allow for control in the opposite direction. Finally, combined control is a combination of these modes, and the right stabilizer will be deflected from the cant angle required for longitudinal trim.

4.2 Longitudinal Control

When using the variable cant stabilizers to control pitch the same requirements as the baseline must be satisfied; the aircraft must be longitudinally stable and trimmable for a useful range of C_L's. Varying the stabilizer cant angle will change the aircraft pitch stability, and the aircraft should be stable for all cant angles. The critical case for stability is cant angles of -90° or +90°. For these cant angles none of the stabilizer is in the horizontal plane, and the aircraft neutral point (NP) will be at the most forward location. A minimum SM of 5% was selected, which results in a CG location at 20% MAC. The SM variation with cant angle is shown in Figure 21. The maximum SM occurs at a cant angle of 0°, and is 28%, a rather large SM.

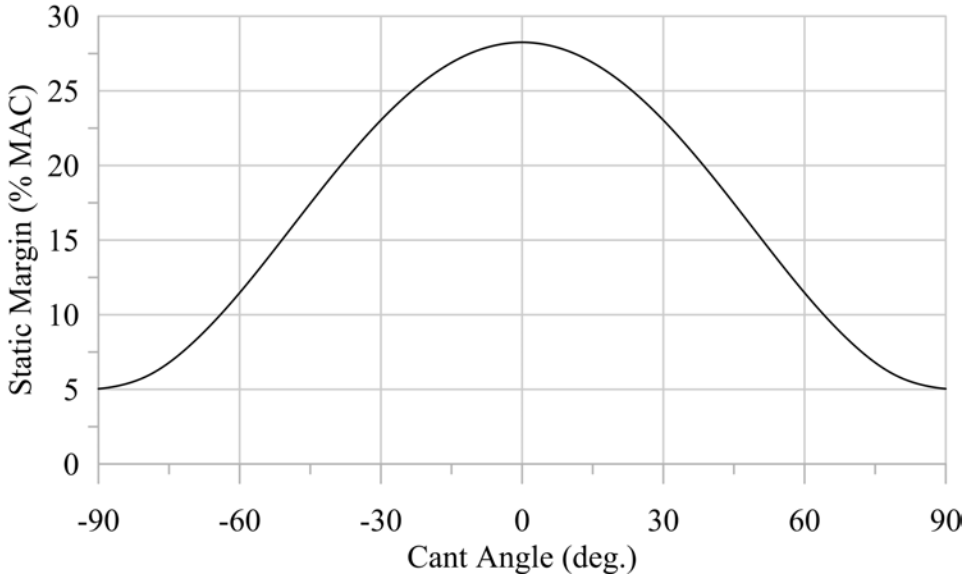

Figure 21. Static margin variation with cant angle.

After selecting the CG location, the aircraft trim is determined. The lift and pitching moment equations from Chapter 2 are solved simultaneously to calculate the trim CL for cant angles ranging from -90° to +90°. All symmetric airfoils are used, which leads to a C_{M_0} of zero regardless of cant angle. This means that the aircraft can only be trimmed at a C_L of zero.

Investigation of equation (15) shows that there are several options for increasing C_{M_0}, and hence trimming at higher C_L's. Three parameters are of primary interest: incidence angle (i_S), toe angle (t_S), and main wing flap deflection (δ_f). These three parameters are adjusted until it is possible to trim the aircraft at the predicted $C_{L_{max}}$ of 0.8. These results are shown in Figure 22.

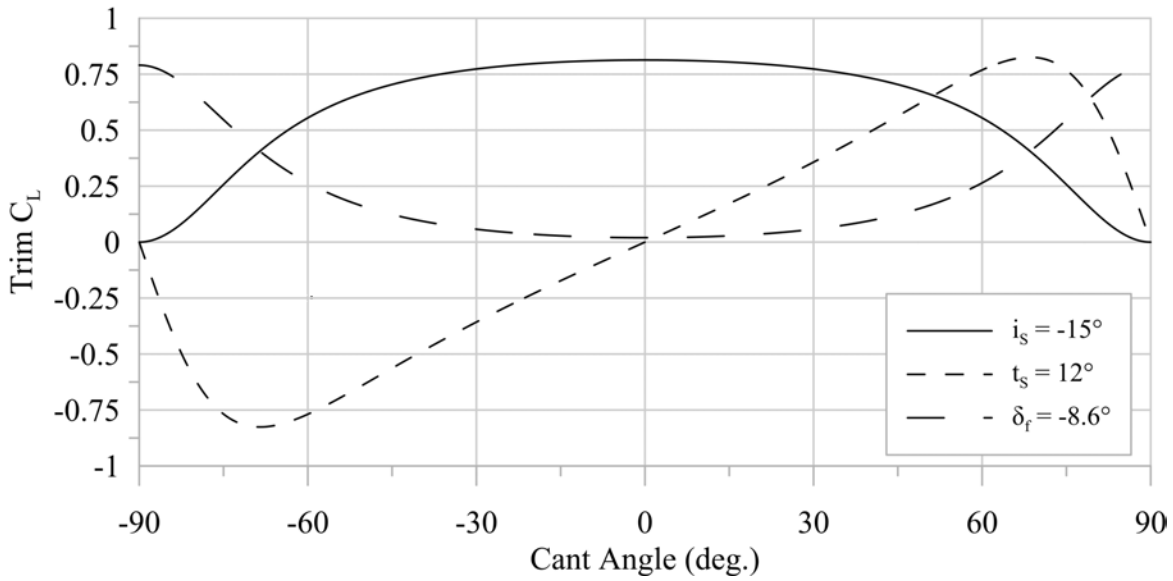

Figure 22. Trim C_L variation as function of cant angle with incidence, toe, and flap settings.

A stabilize incidence angle of -15° is required to achieve $C_{L_{max}}$. This angle is a rather large and the stabilizer may stall (especially at low Reynolds numbers). A skew angle of 12° is required and trim is only possible at positive cant angle. A toe angle of -12° also works, but trim is only possible at negative cant angles. Like incidence, the required toe angle is large with stall possible. Using the flap allows the aircraft to trim with a deflection of just -8.6°. This deflection is small and does not have a large impact on aircraft lift or drag. Additionally, future aircraft could utilize a reflexed airfoil to achieve this effect and may require even less or no flap deflection.

While all three options allow for trimming at the predicted $C_{L_{max}}$, using flaps to adjust the C_{M_0} is deemed the most viable, but there are downsides to this configuration. At $C_{L_{max}}$ the lowest effective wing loading would be desirable, but when flaps are used the lowest effective wing loading occurs at low C_L's when the stabilizer cant angle is small. While this is not ideal, there are some possible benefits. At high CL's the stabilizer cant angle will be large, providing more vertical surface and greater lateral-directional stability at low-speeds condition. As the speed increases the

vertical area will decrease, but less yaw stability is usually required at cruise and may be acceptable. At low speeds the more upright stabilizer will also create less loads in the wing, and this may reduce the reinforcement required.

Although trimming at $C_{L_{max}}$ is possible with the flap deflection the aircraft cannot be trimmed below a C_L of zero. Trimming to a C_L below zero is usually not required but reducing the trimmable C_L would limit the required cant angles and preserve more vertical area. Reducing the trim C_L can be achieved by adding incidence angle (i_S) or toe angle (t_S) to the stabilizers, as shown in Figure 23 for δ_f = -8.6°. Both incidence and toe angle can be used to lower the minimum trim C_L, with toe angle allowing the cant angle for minimum C_L to be shifted to a cant angle other than 0°.

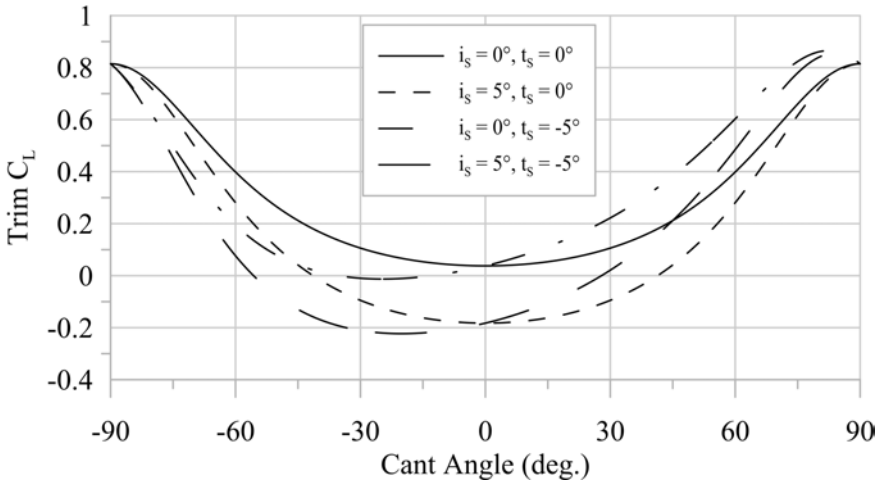

Figure 23. Trim C_L as a function of cant angle with δ_f = -8.6° and incidence and toe angles.

It is worth noting that changing the stabilizer area, used in combination with incidence or toe angle, can also change the C_{M_0}. However, this also increases the SM, which reduces the trimmable C_L. A small stabilizer area study was completed but found not to improve the aircraft trim. The stabilizer area may not be the optimal area but should produce a viable aircraft.

The results from the simple analytical model indicate that a small main wing flap deflection, in combination with a small stabilizer incidence angle, provide the most viable option for longitudinal trim and control. After narrowing down the variables of interest, OpenVSP was used to analyze the configuration with more detail. The OpenVSP model was the same as the baseline aircraft, but with "Hinges" added that allowed the stabilizer cant, incidence, and toe angles to be easily adjusted. The OpenVSP model is shown in Figure 24, with the "Hinges" represented by circles on the stabilizer root leading edge.

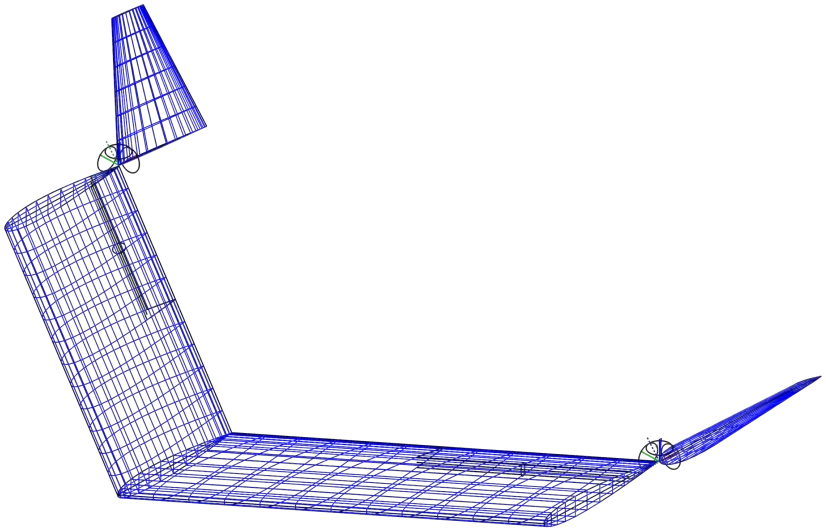

Figure 24. OpenVSP model of variable cant configuration.

OpenVSP predicted a neutral point 6.1% further forward than the simple analytical model, requiring the CG location to be shifted to 13.5% MAC, for a SM of 5.4% with a cant angle of 90°. A flap deflection of -10° was required to reach a $C_{L_{max}}$ of 0.8, however it was not possible to trim at this $C_{L_{max}}$ with incidence angle alone. With -15° incidence the maximum $C_{L_{max}}$ was possible was only 0.55, well below the maximum C_L possible. Decreasing the incidence angle further will almost certainly cause stabilizer stall, so it was not considered.

While a $C_{L_{max}}$ of 0.8 was possible with flaps, it was only possible to trim to a minimum C_L of 0.2. An incidence angle of 5° can be used to reduce the trim CL to 0, which should provide sufficient control. The incidence angle can be increased further to reduce the necessary cant angle range if desired.

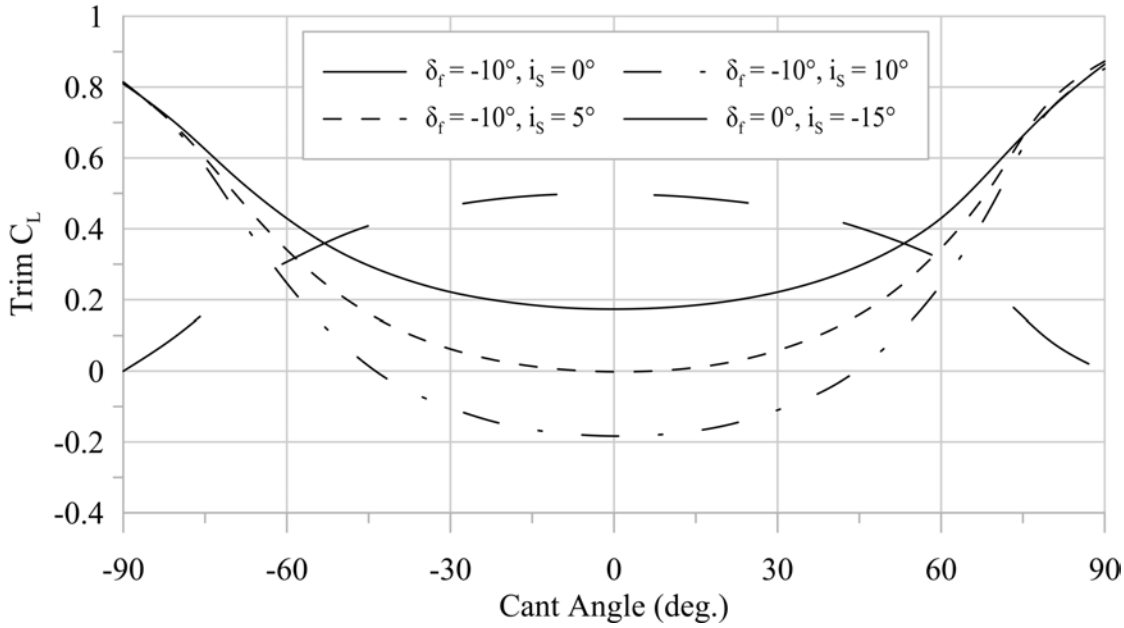

Figure 25. Trim C_L variation as a function of cant angle for several flap and incidence settings.

4.3 Lateral-Directional Control

When analyzing the flying wing Bourdin [7], [8] utilized a scheme where one stabilizer would remain fixed at 0° cant angle, and the other stabilizer would be deflected to generate rolling and yawing moments. The same method was applied to the B&V configuration, but before the rolling and yawing moments were calculated a suitable CG location needed to be determined. Only one stabilizer will be deflected at a time which allows the CG location to be further aft than for longitudinal control. The CG is set at 33.8% MAC giving a SM of 5% with one stabilizer deflected, and 15% with both stabilizers at 0° cant angle. The rolling and yawing moments for a right stabilizer deflection are shown in Figure 26.

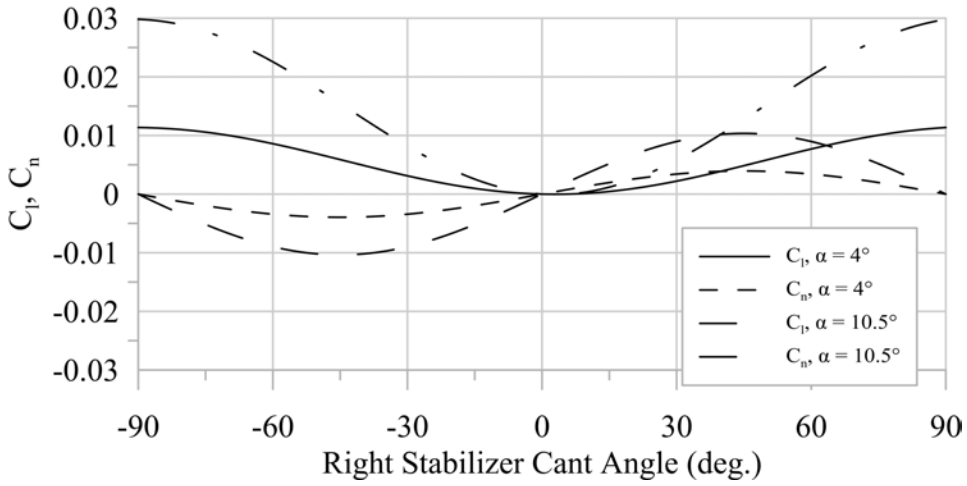

Figure 26. Rolling and yawing moments with left stabilizer fixed at 0° cant.

When the right stabilizer has a positive cant angle proverse yawing moments are generated and negative cant angles generate adverse yawing moments. Although proverse yaw is possible, maximum rolling and yawing moments do not occur at the same cant angles, with maximum rolling occurring at +90° and -90°, while yaw occurs at -45° and +45°. The rolling and yawing moments are also dependent on the aircraft angle of attack. At zero angle of attack no rolling or yawing moments are generated, regardless of cant angle. As the angle of attack is increased, the rolling and yawing moment increases. At low-speed, high-C_L conditions the aircraft will be much more maneuverable than at high-speed, low-C_L conditions.

In this configuration main wing control surfaces are used as elevators. Trim C_L as a function of elevator deflection is shown in Figure 27. With the selected CG location the aircraft can only be trimmed to a C_L of 0.55 with -30° of elevator deflection. This is well below the aircraft $C_{L_{max}}$, and would severly limit the aircraft's low-speed performance. If the CG is shifted aft so that the aircraft can trim at $C_{L_{max}}$ with δ_e = -20°, then deflecting one stabilizer to 90° cant angle results in the aircraft becoming unstable.

Figure 27. Trim C_L as a function of elevator for lateral-directional variable cant configuration.

Another consideration of using the stabilizer for lateral-directional control is the rolling and yawing moment magnitude generated. From the OpenVSP results for the baseline aircraft an aileron deflection of 10° generates a rolling moment of 0.052. The maximum rolling moment using the variable cant stabilizers was found to be 0.044, which occurs at an angle of attack of 10.5°. At lower angles of attack the rolling moment is reduced even further and may not provide adequate roll and yaw control.

Having both stabilizers at +90° or -90° when not maneuvering was also investigated but had similar problems. While the aircraft can be easily trimmed not maneuvering, deflecting a stabilizer increased the static margin, and made the aircraft un-trimmable with one deflected. All of these conditions were also checked in OpenVSP and showed similar results. The difficulties of trimming the aircraft, combined with the small rolling and yawing moments make the stabilizers a poor choice for aircraft lateral-directional control.

4.4 Combined Control

While varying the stabilizer cant angle can be used to control the aircraft longitudinally additional control surfaces are required for complete control of the aircraft. If the stabilizers could

be used to simultaneously control the aircraft both longitudinally and lateral-directionally than the number of actuators required could be reduced, reducing weight and increasing simplicity.

To use the stabilizers for combined control the longitudinal trim requirements must first be satisfied. Using a small negative flap deflection with small positive stabilizer incidence angle provided the best longitudinal control, with the largest trim range possible. These settings allow trim at either positive cant angles or negative cant angles. Analysis shows that if the negative cant angle range is used then proverse yaw is possible, so this range is selected.

For trim C_L's bellow $C_{L_{max}}$ the cant angle must be reduced and the lateral-directional control at these trimmed cant angles needs investigation. The cant angle is set in the OpenVSP model, and then the angle of attack is adjusted so that the aircraft is trimmed in pitch. Once trimmed the right stabilizer is deflected in the positive direction, up to 45°, from the trimmed cant angle. The results for trimmed C_L's of 0.81, 0.34, 0.06, and 0.0 are shown in Figure 28.

As the trimmed C_L is reduced the rolling and yawing moment magnitude reduces significantly, the same as pure lateral-directional control. At the maximum C_L the stabilizers also generate proverse yaw, but at any other C_L the stabilizers generate adverse yaw, if any significant yawing moment are generated at all. Additionally, at a C_L of 0 right stabilizer deflection creates a rolling moment in the opposite direction as the other higher C_L's. This will create a reversal in the aircraft's response to pilot input and would be difficult to fly and are not likely to provide reasonable control.

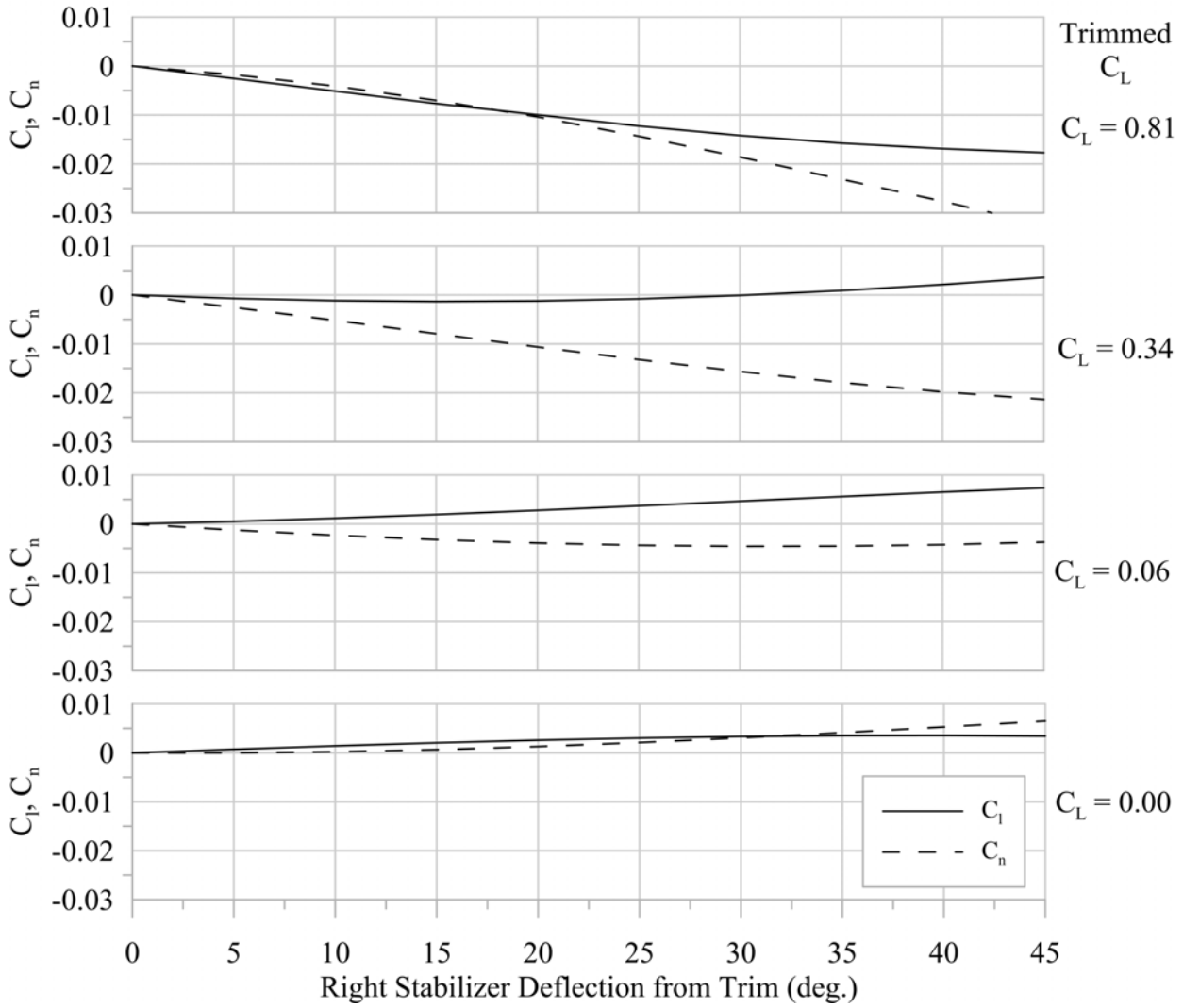

Figure 28. Rolling and yawing moments at several trim C_L's.

4.5 Performance

Finally, the cant angle effect on aircraft performance was analyzed. The lift-to-drag ratio (L/D) for several cant angles is shown in Figure 29. The results show that 0° cant provides the maximum lift-to-drag ratio and increasing cant, in either the positive or negative directions, lowers the L/D. Interestingly, negative cant angles all have higher L/D ratios then the equivalent positive cant angles, likely due to the effect of wing tip vortices. The L/D for a cant angle of -20°, the cant angle of the original B&V design, was also checked. This cant angle actually provides the largest

L/D, slightly greater than even 0° cant. Clearly the designers selected the cant angle for maximum performance, and not for stability reasons.

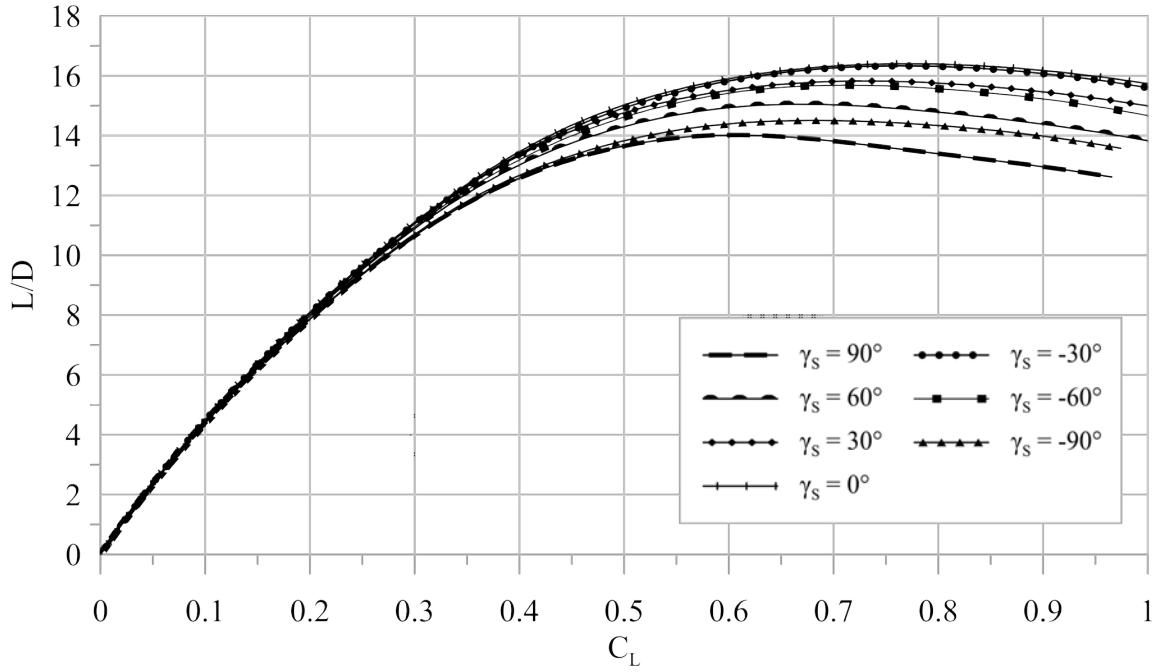

Figure 29. Lift-to-drag ratio as a function of C_L for several cant angles.

These results show which cant angles will provide the maximum L/D, but this analysis did not incorporate any effects of trim. When the cant angle is used to control the aircraft in pitch the cant angle will be constantly varied. The drag due to control surface deflection should also be considered, as this may have a large impact on aircraft drag. Three different configurations are analyzed: the baseline configuration, variable cant with -10° of flap deflection and 5° of incidence, and variable cant with -15° of incidence. Additionally, the increase in parasite drag due to flaps was estimated using the model given in Roskam [19]. The results of this analysis are shown in Figure 30. The results indicate the baseline aircraft has a slightly higher L/D for the entire C_L range, and the maximum L/D occurs at a lower C_L than for the variable cant configurations. The variable cant configuration with flaps is only 4% lower than the baseline configuration.

It should be noted that neither one of these designs has been optimized, and improvements to both curves may be possible. Even though no large increases in L/D are seen, there may be benefits in control and handling qualities provided by the variable cant configuration. Additionally, maximum L/D may not be the key requirements for all missions, and the variable cant may provide for lower overall drag or lower weight.

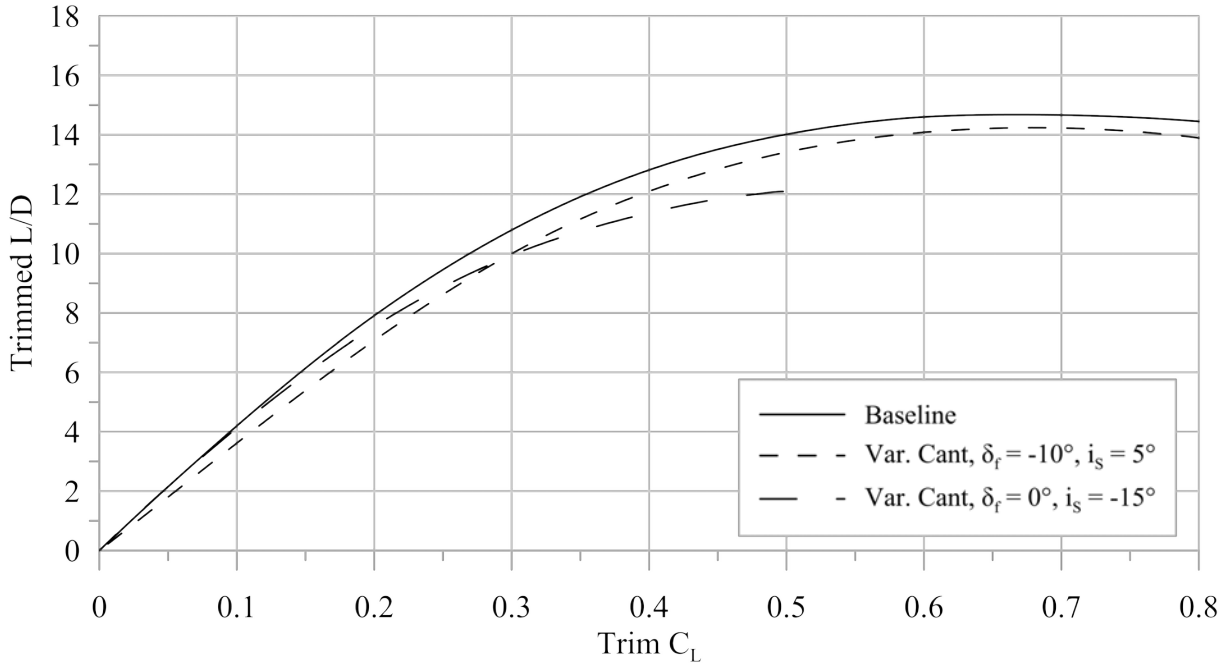

Figure 30. Trimmed L/D for three Configurations.

CHAPTER 5

MODEL

5.1 Configuration Layout

The previous analysis focused on the combination of wing and stabilizer, and the fuselage was not considered. After completing the analysis, the requirement is known and a fuselage layout could be selected. The primary concern is that the model be able to balance at the correct CG location for all configurations. The original B&V design used a pusher configuration, which would work for the baseline. However, the variable cant configuration requires the CG to be much further forward. A weight build-up revealed that achieving this forward CG location would require an extremely long nose section. If a tractor layout is used, then the forward CG location can be more easily achieved without a long nose section.

Additional vertical surface is also required to ensure that all configurations are stable in yaw. While many of the B&V concepts utilized vertical fins mounted at the same location as the stabilizers these would likely impact the testing results and would be more difficult to build. Instead, a model with a single, central, vertical surface is selected. The vertical tail is sized to have a vertical tail volume coefficient of 0.04, which should provide adequate stability. Using a single vertical surface requires lengthening the fuselage to provide a mounting location. This also increases the fuselage internal volume, which allows more room for electronics without requiring the frontal area to be increased.

5.2 Electronics

The electrical and propulsion components used for the model are shown in Table 5. The components were selected to minimize weight while still providing the necessary features. A static thrust of 1.7 lbs was generated with the selected propeller, motor, and battery. Flight times of 6

minutes are possible with the selected battery capacity. Futaba S3114 servos were used for the traditional control surfaces, while the Futaba S3102 servo, which provides a greater torque, was used for the variable cant stabilizer.

TABLE 5

SELECTED ELECTRICAL/PROPULSION COMPONENTS

Battery	Great Planes LiPo 3S, 850mAh, 25C
Motor	Great Planes Rimfire 0.1
Electronic-Speed-Controller	Castle Creations Talon 25A w/BEC
Propeller	APC 9x6E
Servos	Futaba S3114/Futaba S3102
Reciever	FrSky S8R/S6R

5.3 Primary Test Article

The primary test article was built to be used for both wind tunnel and flight testing. The requirements of each must be balanced: lightweight for flight testing, but strong and stiff for wind tunnel testing. Figure 31 shows the aircraft and its three major components; the wing, the stabilizer mechanism, and the fuselage. In addition, the model had to support multiple configurations, and was made with swappable stabilizer mechanisms. A brief description of the design and construction methods used is provided below.

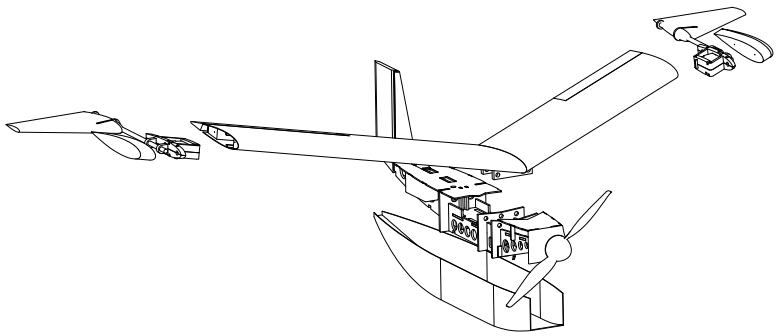

Figure 31. Exploded view of primary test article.

5.3.1 Wing

The wing is constructed using a solid foam core with 1/32” balsa bonded to the surface, providing significant torsional stiffness. Two 1/8” spruce stringers placed on the top and bottom of the wing at the quarter chord location as well as a 3/32” balsa rear spar placed at the three-quarter chord location. Two 1/4” plywood spars are located at the wing root perpendicular to the root chord. This provides strength at the root and allows the fuselage to be attached to the wing using nylon bolts.

The stabilizer mechanism is attached to the wing tip. A pocket is milled into the foam at the wing tip into which the stabilizer mechanism slide. The mechanism also locks onto the stringers and skin, providing a strong connection. The pocket in the wing, without the 1/32 balsa skin attached, is shown in Figure 32. Threaded brass inserts are also bonded into the wing tip to allow the stabilizer mechanism to be bolted to the wing tip. Vacuum formed pods are then taped onto the wing tip to cover the rotation mechanism and reduce drag.

Figure 32. Wing core with stabilizer mechanism installed.

5.3.2 Stabilizer Mechanism

Only one wing would be built, so the stabilizer mechanism had to be modular to support testing of multiple configurations. The parts are also made to be accessible to allow easy replacement. An exploded view of final design for the variable cant stabilizer mechanism is shown in Figure 33. The mechanism consists of two 3D printed frames which are bolted together using nylon screws and heat set threaded inserts. When the two halves are bolted together the servo and the stabilizer pivots are locked into place. The pivots can be easily replaced to create any incidence or toe angle desired.

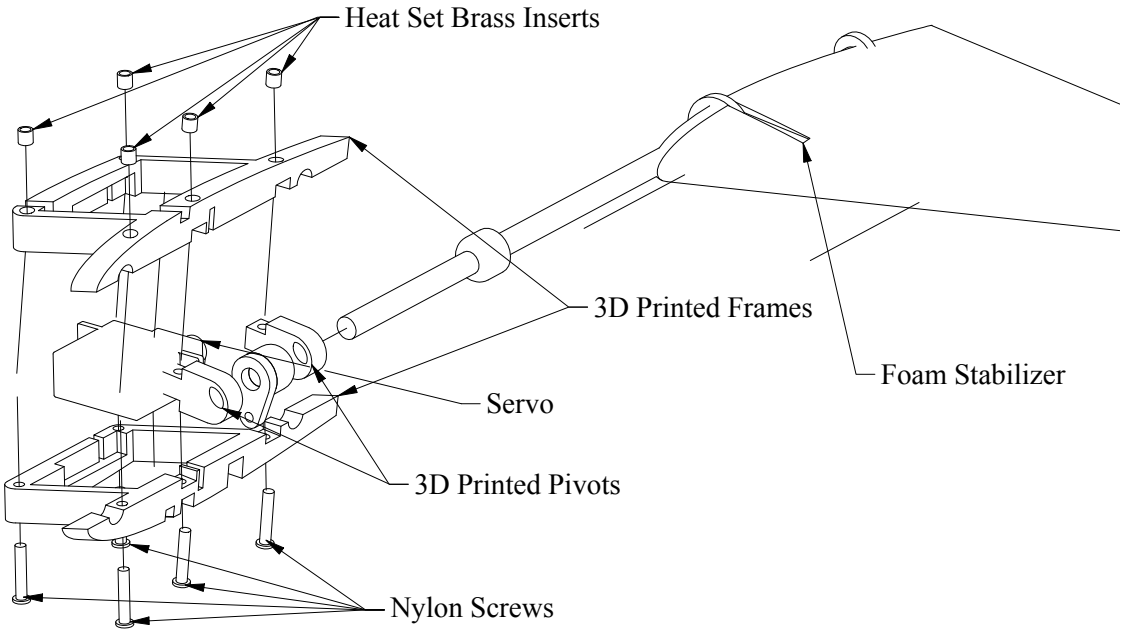

Figure 33. Exploded view of stabilizer mechanism.

5.3.3 Fuselage

The fuselage needed to be able to hold a variety of electronic systems that need to be shifted around to allow adjustment of the aircraft's CG. Interlocking 1/8" plywood panels were used for the forward portion of the fuselage, while balsa was used for the aft portion. The fuselage had two

bulkheads that allow the fuselage to be bolted to the cross members in the wing. A 1/32” balsa shell was constructed to provide a clean aerodynamic profile for the fuselage. The aircraft with the balsa shell removed is shown in Figure 34.

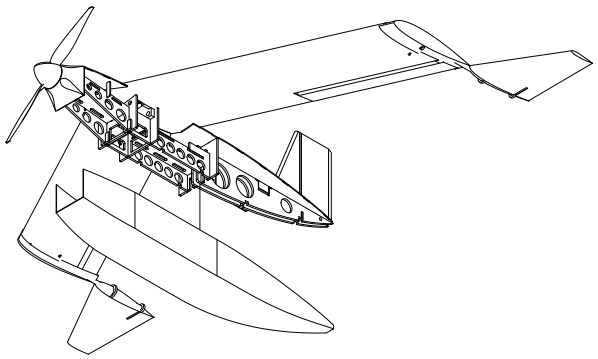

Figure 34. Aircraft with fuselage cover removed.

5.3.4 Completed Model

The completed aircraft ready to fly is shown in Figure 35. A three-view of the variable cant configuration with key dimensions is shown in Figure 36.

Figure 35. Completed primary test article.

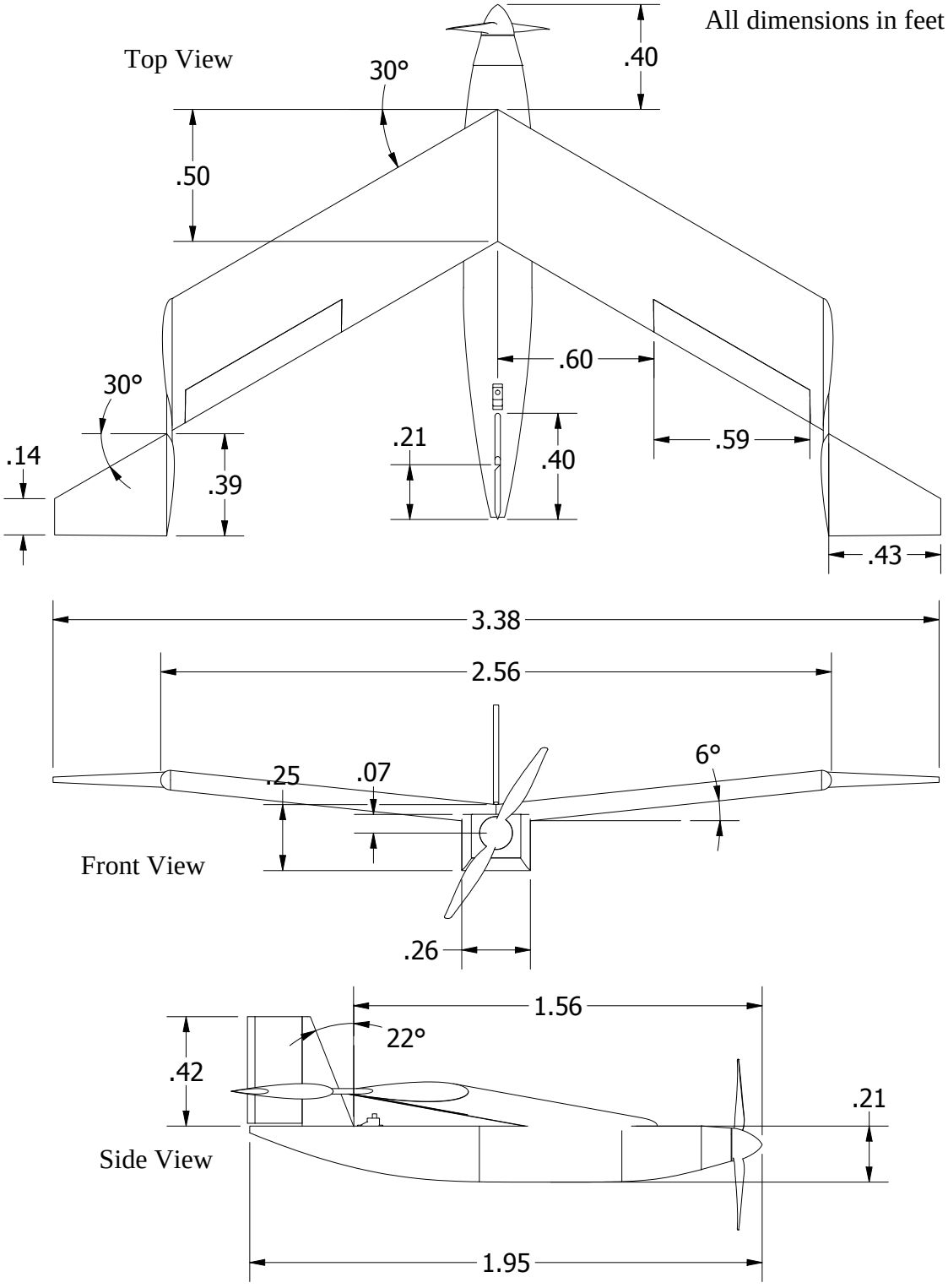

Figure 36. Aircraft three-view with key dimensions.

5.4 Foamie Model

A second version of the baseline aircraft, called a foamie (shown in Figure 37), was also constructed to allow extensive test flying without risking damage to the primary test article. It was built using the same dimensions of the primary test article but employed different methods which made it quicker to build. The primary test article, while well suited to wind tunnel testing and normal flight operations, was not robust enough to handle hard landings or crashes and would require extensive repairs if crashed. The foamie did not have this issue and was more robust for test flying. Although more robust for test flying, building the variable cant stabilizer configuration using this method would be very difficult. Additionally, the construction methods used would not handle the loads in the wind tunnel.

The wing was made from solid foam, with a 1/8” basswood spar located at the quarter chord, then covered in 3 mil laminate. The stabilizers where bonded to the wing tip at the baseline cant angle and were also covered in laminate. Foam is bonded to either side of a 1/4” plywood keel structure to construct the fuselage. Pockets are milled out of the foam to allow for the placement of the various electronics. Initially the foamie was only a glider, but later a 1/4” plywood bulkhead is bonded to the front of the foam and the motor is bolted to this bulkhead to allow powered flight.

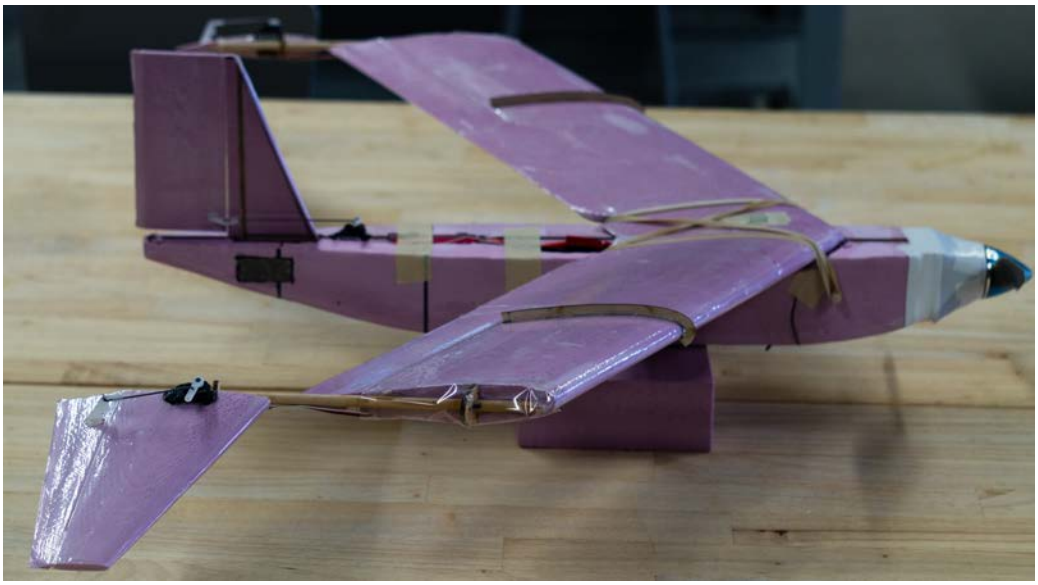

Figure 37. Completed foamie model.

CHAPTER 6

WIND TUNNEL RESULTS

6.1 Apparatus

Wind tunnel testing was performed in the Wichita State 3 ft x 4 ft Low-Speed wind tunnel, shown in Figure 38. It is an open return type tunnel with two test sections, a 7x10 ft section capable of dynamic pressures up to 0.75 psf, and a main test section is 3x4 ft, and is capable of dynamic pressures up to 25 psf. A three-component balance is mounted above the main test section which can measure lift, drag, and pitching moment, and models are typically mounted in the tunnel inverted. The balance has the following limits and uncertainties:

Lift = 50 lbs ± 4% fs

Drag = 25 lbs ±1.2% fs

Pitching Moment = 8 lbs-ft ± 3% fs

Angle of Attack = -14° to 22° ± 0.25°

Dynamic Pressure = 25 psf ± 0.05% fs

Figure 38. 3x4 Wind tunnel and model instillation.

The WSU 3x4 LSWT balance cannot measure lateral-directional forces and moments, hence the vehicle the predictions of these forces are not validated. The data outputted by the wind tunnel is reduced to coefficient form, and then the moments are adjusted to the aircraft's CG. No corrections (e.g. blockage, buoyancy, etc.) are made to the wind tunnel data; however, the model is small compared to the test section and the corrections are likely to only have a small impact on the results.

6.2 Testing Conditions

A cruise speed of 60 ft/s was chosen for flight testing. This is a sufficient speed to handle windy conditions and maximizes battery endurance for flight testing. Using this speed and the chord as the reference length gives a Reynolds number of 200,000. All wind tunnel data presented was tested at this Reynolds number unless otherwise noted. An angle of attack range from -8° to 20° was tested, with data taken at every 2°. Baseline elevator data was taken at 10°, 0°, -10° and -20°. Main wing flaps were run at -7.5°, and -10°. For variable cant runs the stabilizer cant angle were: -82°, -60°, -30°, 0°, 30°, 60°, and 82°.

6.3 Baseline Configuration

6.3.1 Longitudinal Forces and Moments

The baseline configurations' lift, drag, and pitching moment with no elevator deflection is shown in Figure 39. The results show good correlation with the predictions, with two notable exceptions. First, at angles of attack above 8° significant non-linear effects are observed in the lift, drag, and pitching moment. Most concerning is the unstable pitching moment break and may create issues in flight. Secondly, at angles of attack bellow 8° the pitching moment does not match predictions, with a larger C_{M_α} seen in the wind tunnel than OpenVSP predicted. Investigations were made to determine the cause of these differences.

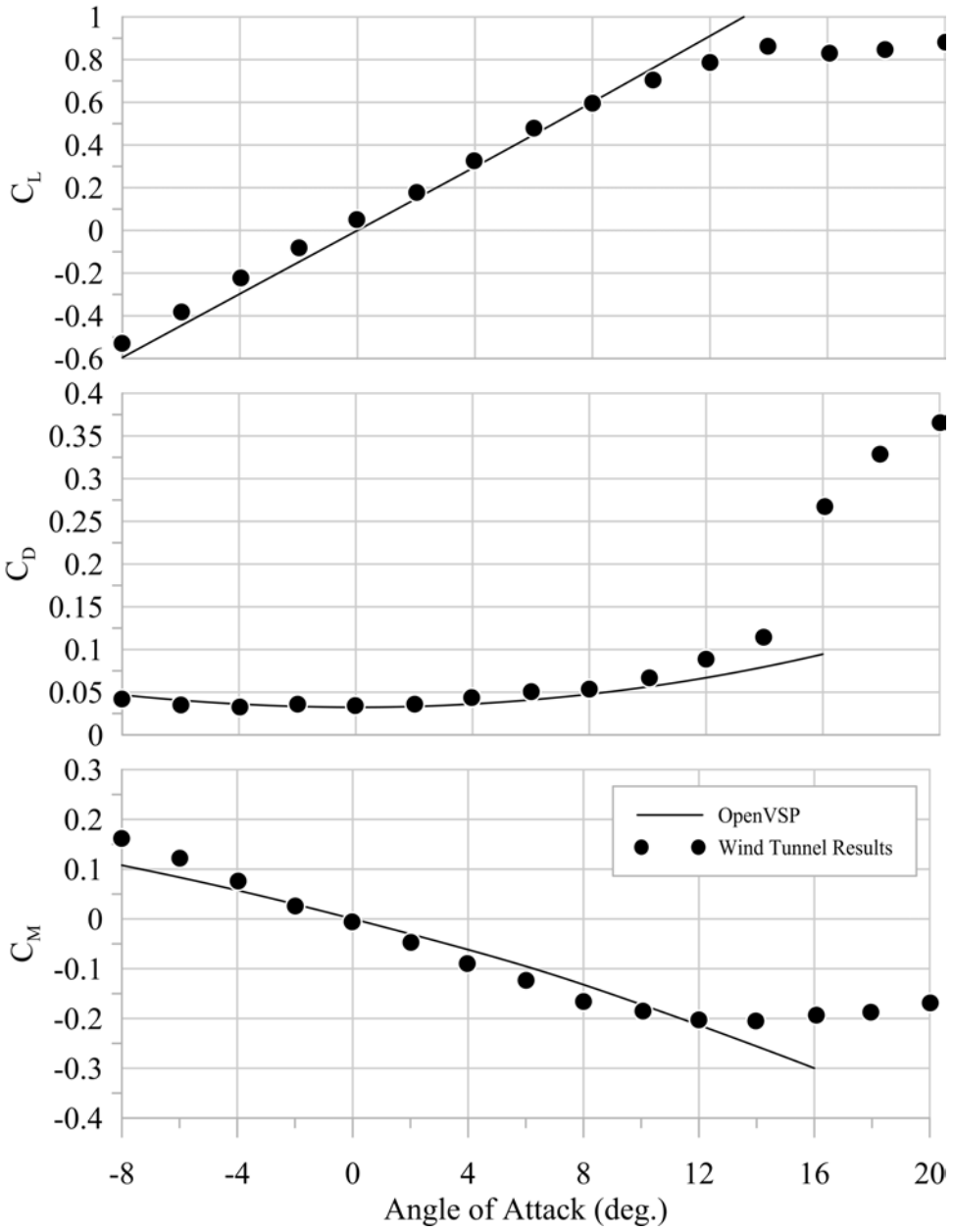

Figure 39. Wind tunnel results for baseline configuration with no elevator deflection.

6.3.2 Tip Stall Effects

The non-linear affects are believed to be caused by tip stall, a common occurrence on highly swept wings. Flow-visualization was used to confirm this suspicion. One half of the model was tufted, with a row at the LE and one at the quarter chord. The tunnel was run at the same

conditions as the data runs. At angles of attack above ~10° severe wing tip stall is observed, shown in Figure 40. Tip stall causes the wing AC to shift forward, reducing aircraft static stability. At angles of attack above 12° this effect causes the aircraft to become unstable.

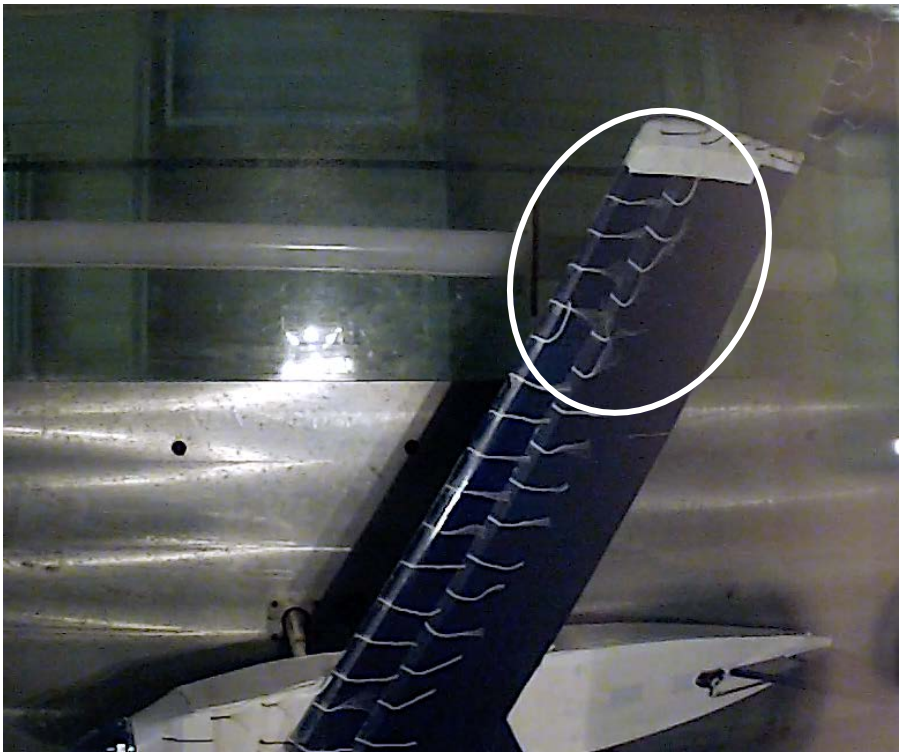

Figure 40. Top View of tufted wind tunnel model at an angle of attack of 12°.

Preventing this tip stall will make the aircraft much easier to fly and less prone to crashing. Typically, washout is used on swept wings to prevent tip stall, but this is not an option as the model has already been constructed. Two tip stall prevention devices were tested: a wing fence and leading-edge extensions (LEX). The wing fence was sized using Bandettini [20] as a reference. The height was 4% of the wing chord and extended from 10% chord location on the bottom to 75% chord location on the top. They were placed at the 40% span location, the boundary of the stalled boundary at 12° angle of attack. Sizing of the LEX was taken from Lennon [21] and extended the leading edge 3% while maintaining the LE radius. They covered 30% of the wing

span, with the inboard edge at 65% of the span. The wing fences and LEX installed on the model are shown in Figure 41 and Figure 42, respectively.

Figure 41. Wing fences installed on primary test article.

Figure 42. Leading-edge extensions installed on primary test article.

Results for the pitching moment with the tip-stall prevention devices are shown in Figure 43. Both options work to prevent the major effects of tip stall, although neither is ideal. The LEX still has non-linear effects between 12° and 16°, and shows a slight increase in the pitching moment at 14°. The wing fences work even better, with only a slight reduction in the slope of C_{M_α} seen after 12°. Wing fences were added to the flight test model after being tested and performed well.

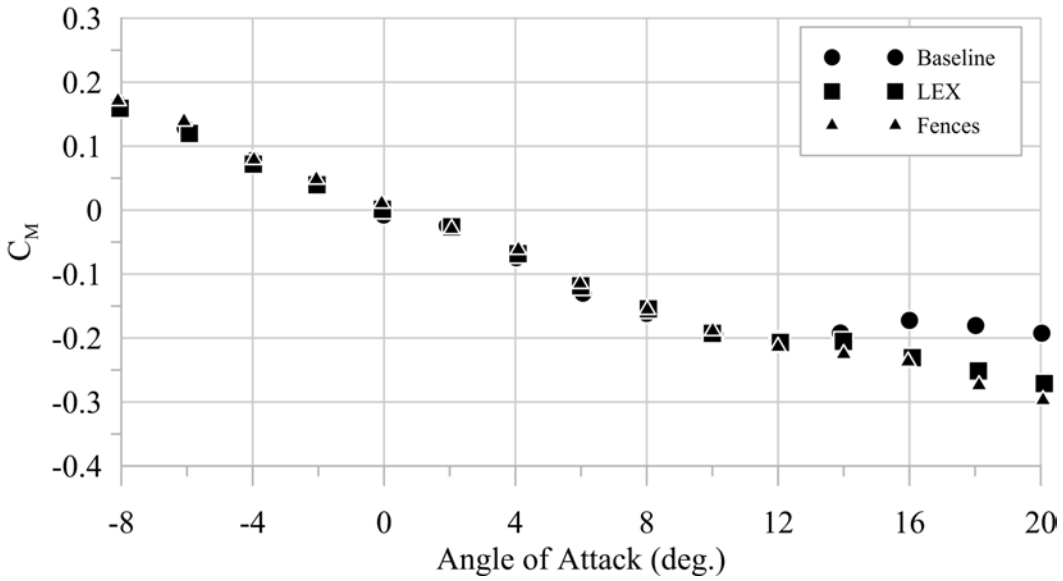

Figure 43. Effect of tip-stall prevention devices on aircraft pitching moment.

6.3.3 Low-Reynolds Number Effects

At low-Reynolds numbers viscous effects are large, however, OpenVSP cannot predict viscous effects, and this may explain the deviations seen at moderate angles of attack. Pope et. al. [22] gives a method for increasing the effective Reynolds number by use of trip strips, and these are used to investigate the low-Reynolds number effects. Pinking shears were used to cut painters tape, and four layers, with total thickness of 0.0128", were placed at the 10% chord location on the top and bottom of the wing and stabilizers, shown in Figure 44. The trips were tested with a cant angle of 0°, with the results shown in Figure 45. The trips strips improve the results for the pitching moment, with a better match in the linear angle of attack range. However, the results for the lift are worse with trip strips, with a lower C_{L_α}than with no trip strips. The model was also tested with 80 grit sandpaper cuffs that extend over the first 10% chord of the wing, with the same results as the trip strips.

Determining the exact impact of low-Reynolds number effects is difficult, and other factors may be impacting the results. The NACA 0015 airfoil used is sensitive to Reynolds numbers, and

may not be corrected by trip strips alone. Although great care was taken while constructing the model, small errors are inevitable, and may be the cause of some of the deviations seen. While the exact cause of these deviations is not known, they do not have a significant impact on the aircraft's stability and performance and are not investigated further.

Figure 44. Wind tunnel model with trip strips installed.

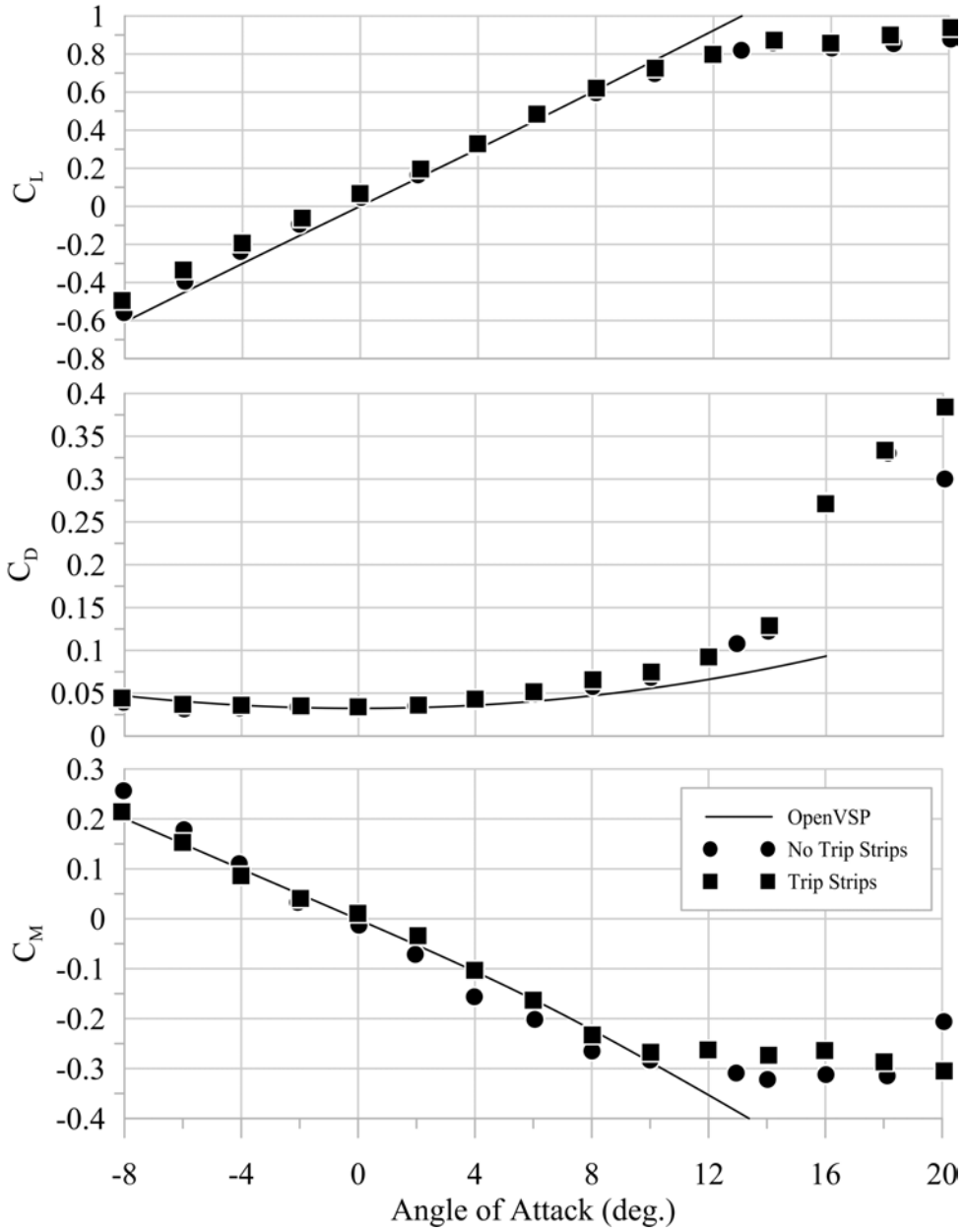

Figure 45. Effect of trip strips on wind tunnel results.

6.3.4 Baseline Trim

The baseline configuration's trim capabilities were also investigated. Four different elevator deflections were tested: 10°, 0°, -10°, and -20°. Due to the pitching moment deviations the model has a SM of 30%, which is much larger than predicted. This increased SM reduces the maximum trimmable C_L to 0.35, half of what was predicted. To counter act this the CG is shifted

from 31.5% MAC to 36.6% MAC which provides a static margin of 16%. A trim plot with this CG location is shown in Figure 46. This CG allows the aircraft to trim at a C_L of 0.6 with $\delta_e \approx$ -12°. The data also shows that if the elevator deflection is too large then the aircraft will not trim before the unstable pitching moment break is reached, as can be seen with the elevator deflection of -20°. Flying with the wing fences may correct this issue, but the useable C_L range is limited to 0.6.

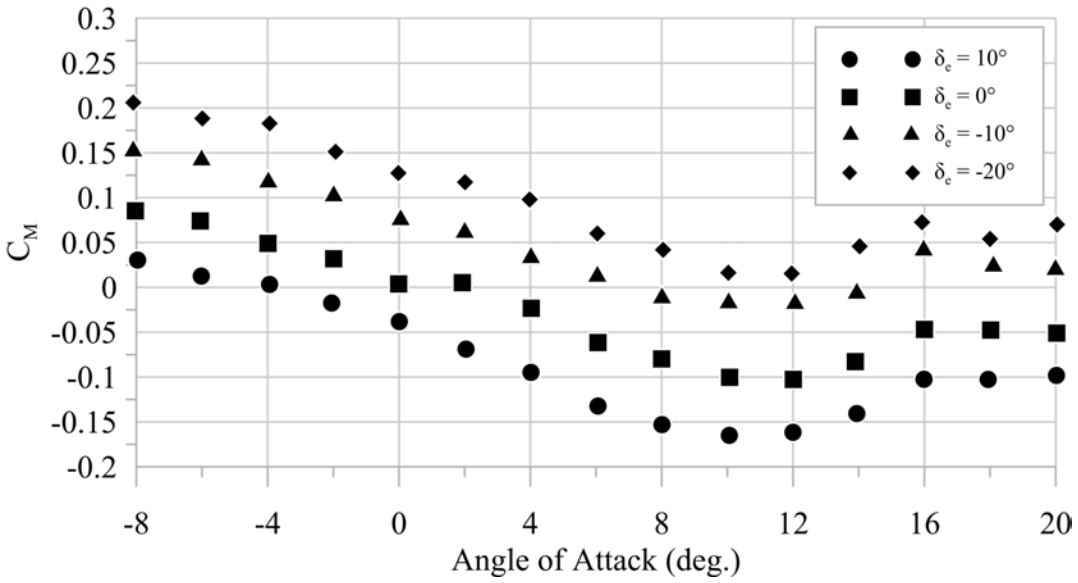

Figure 46. Trim plot for baseline with CG at 36.6% MAC

6.4 Variable Cant Longitudinal Trim

Several cant angles were tested, both with and without flaps deflected. Similar increases in static margin due low-Reynolds number effects were observed for the variable cant configuration, so the CG was shifted from 20% MAC to 23.5% MAC. The wind tunnel results were interpolated to determine the trim C_L for each cant angle tested. OpenVSP predicted a flap deflection of -10° was required for trim while the wind tunnel results showed that only -7.5° was required. The results are shown in Figure 47 and match OpenVSP predictions well. The variable cant has the same tip stall as the baseline, and the pitching moment break is reached before the aircraft can trim for cant

angles of -82° and +82°, so the trim values shown for these values can only be reached if the aircraft is flown with wing fences.

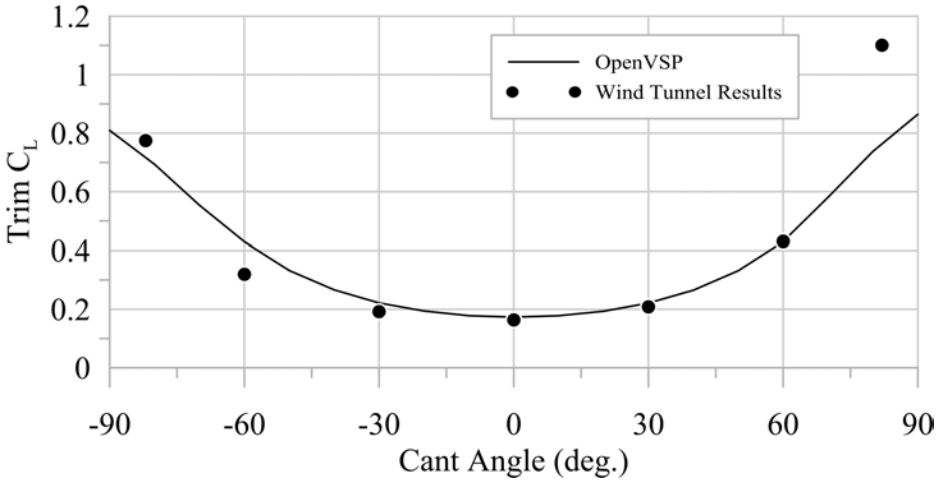

Figure 47. Trim C_L as a function of cant angle from wind tunnel results.

The model was also tested with a stabilizer incidence angle of 5°. The test was completed with no flap deflection, but the change in pitching moment due to flaps was found from previous results and applied to this data, which is shown in Figure 48. These results match the OpenVSP predictions almost exactly, and trim with the variable cant stabilizers should be achievable in flight. Although only the longitudinal forces and moments were measured OpenVSP was able to predict the results reasonably well, and this provides some confidence that the lateral-directional forces and moments are also potentially correct.

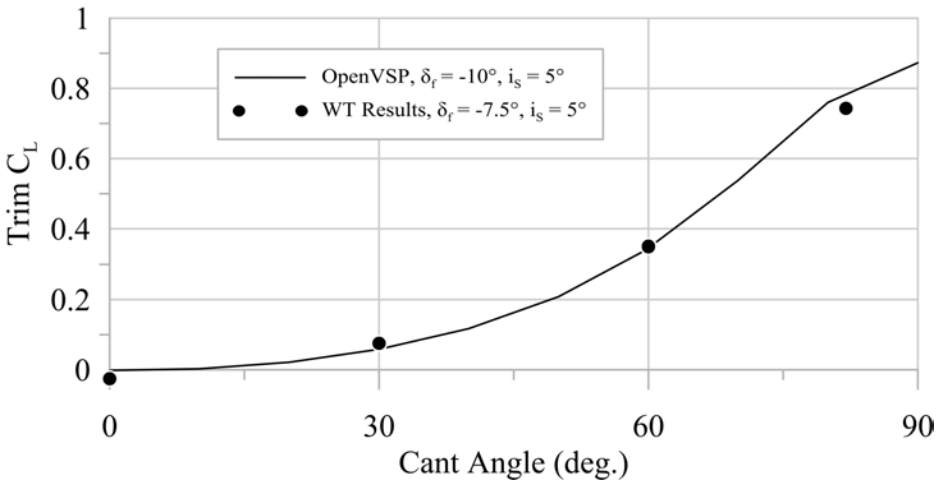

Figure 48. Trim C_L as a function of cant angle with incidence of 5° from wind tunnel results.

6.5 Performance

The L/D for several cant angles from the wind tunnel testing is shown in Figure 49. At low C_L values before separation and non-linear effect the same trends predicted by OpenVSP are seen. However, at higher C_L's the results differ significantly. This difference is likely due to the very large increases in drag at angles above 8°. This causes the L/D to be lower than predicted for all cant angles, and also result in most of the cant angles having the same maximum L/D. At lower C_L conditions a cant angle of 0° still provides the maximum L/D, just as OpenVSP predicted. Trim at low C_L's occur at low cant angles, which will provide the maximum L/D. At higher C_L's the cant angle will be larger, but unlike the OpenVSP results there is not a large difference in the L/D at these high C_L's. This indicates that while it may not be higher, the decrease in L/D is not as large as predicted.

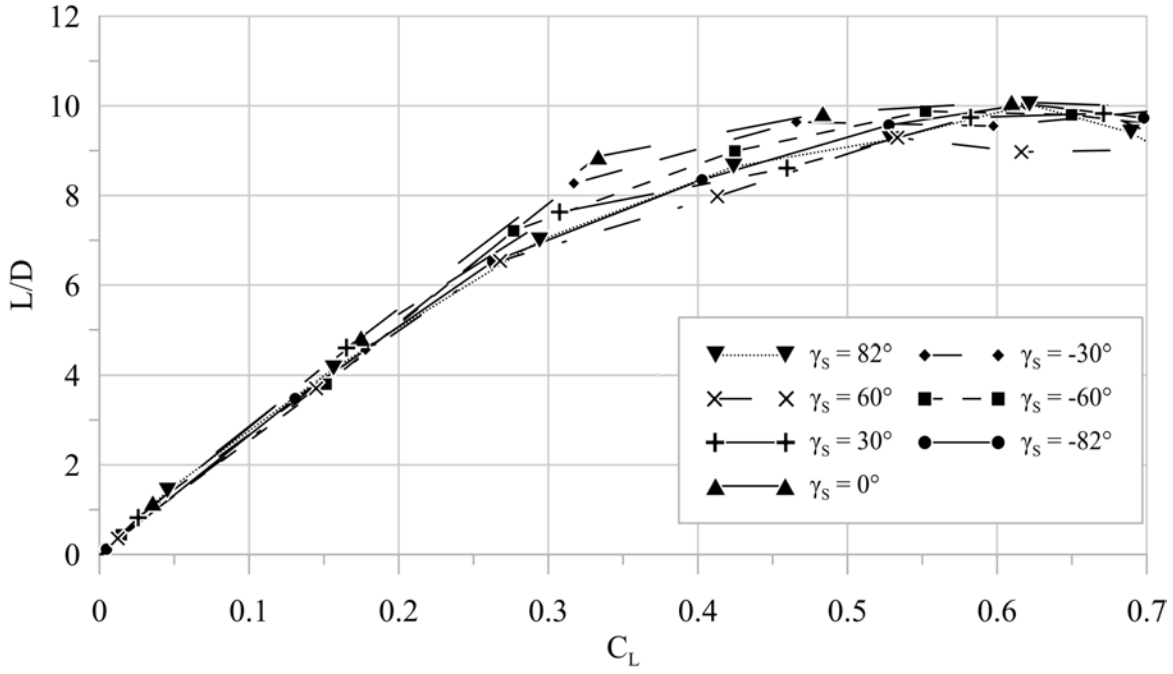

Figure 49. Lift-to-drag ratio for several cant angles based on wind tunnel results.

6.6 Power Effects

During flight testing it was observed that there was a large change in aircraft pitching moment when the model was powered. The model was wind tunnel tested with the same propulsion system used for flight testing installed to determine the precise effects. The results for 100% throttle at 40 ft/s, the aircraft's stall speed, is shown in Figure 50. Throttle up causes a change in both $C_{M_0}$and C_{M_α}. The change in C_{M_0} is due to thrust line being below the CG, creating a nose up pitching moment. The change in C_{M_α} is likely due to increased airspeed over the wing center portion, causing the wing AC to shift forward. This results in a SM reduction of 6% making the aircraft less stable. The test was also performed at the cruise speed, with the same change in SM observed, but no change in C_{M_0}, due to the decreased thrust at high speeds.

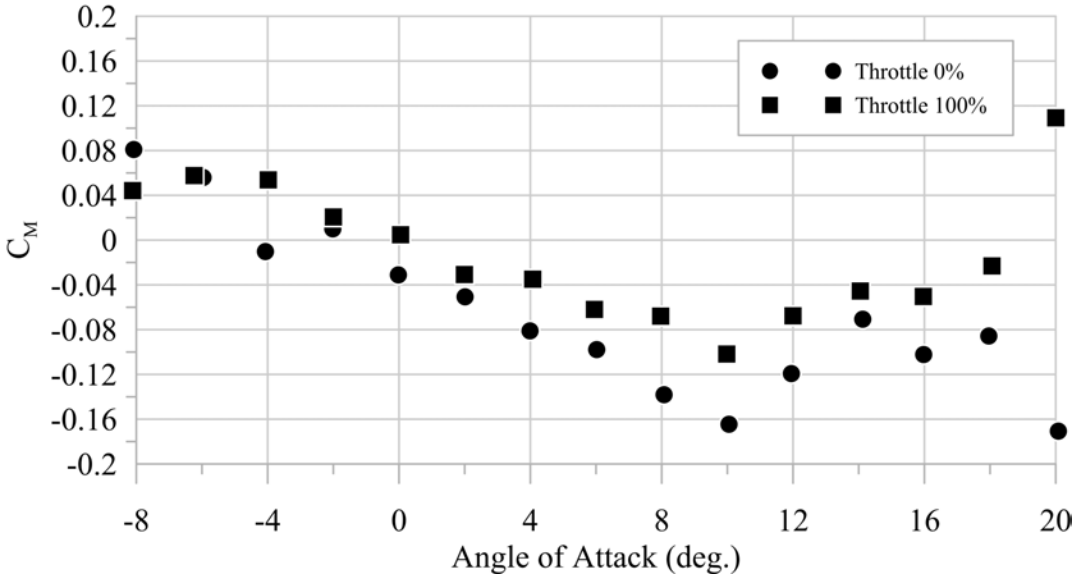

Figure 50. Effect of motor and propeller on aircraft pitching moment.

CHAPTER 7

FLIGHT TESTING

7.1 Baseline Configuration

The baseline configuration was flown first, before attempting any variable cant flights. Figure 51 shows the control surface layout used for the baseline aircraft. Initial flight weight was 1.61 lbs, and was later reduced to 1.42 lbs. The CG location was set at 39.8% MAC for the initial flights, and later adjusted to 36.6% MAC. The reasons for the CG and SM changes are discussed in the following sections.

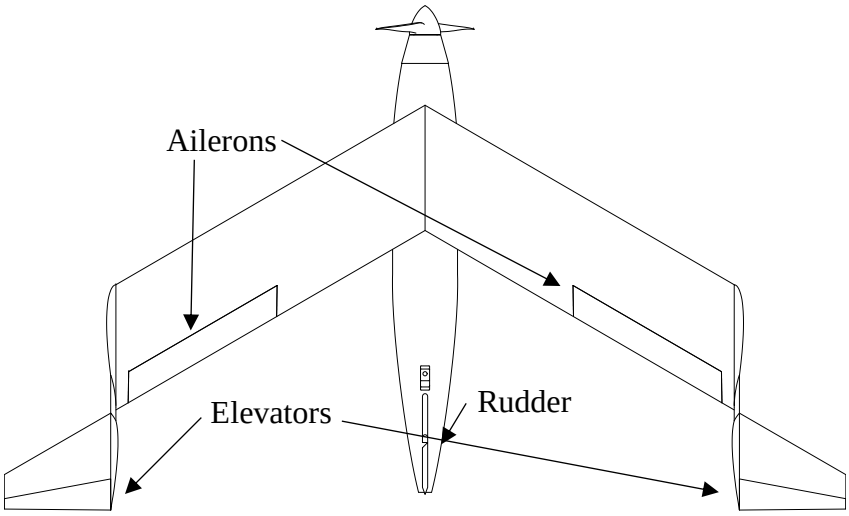

Figure 51. Baseline aircraft control layout.

7.1.1 Initial Flight Attempts

Before beginning flight testing there was concern over the unstable pitching moment break, but it was felt it would be possible to avoid this unstable region. However, this proved to be incorrect, with severe instability seen immediately after launch in the first several flight attempts. Analysis of video and available flight data revealed the aircraft reached a large pitch angle, and it

is suspected that the angle of attack exceeded the range where the aircraft was stable and became unstable.

7.1.2 Glider Flights

After the difficulties flying the main test article a foamie glider was constructed. This was built to allow the pilot the opportunity to practice the bungee launch, as well as determine why the main test article did not behave as expected, without risking damage to the primary test article. This aircraft did not contain a propulsion system so ballast was added to ensure that the weight and CG location matched the primary test article. The aircraft in the process of being bungee launched is shown in Figure 52.

Figure 52. Foamie glider being bungee launched.

The glider flights proved highly successful, with over a dozen successful flights. These flights validated the selected CG location, with the aircraft displaying sufficient pitch stability, and control authority. After the successful flights the pilot attempted to force the aircraft into a tip stall to recreate the instability observed for the primary test article. However, the same instability was not observed. When the pilot commanded a nose up pitching moment it caused the glider to slow

down significantly, which forced a stall on the entire wing and the aircraft pitched down, rather than becoming unstable.

7.1.3 Foamie Model Flights

After the glider flights proved successful, a propulsion system was added to the foamie aircraft to allow testing of a powered model, which is shown in Figure 37. The aircraft was again ballasted and balanced to the same CG location and weight as the main test article. The aircraft was bungee launched and allowed to glide for a few seconds and demonstrated sufficient pitch stability. The pilot then eased up to full throttle and the aircraft pitched up dramatically until it was vertical, then the aircraft began tumbling, displaying the same instability seen with the main test article. The pilot then throttled all the way back down, and the aircraft became noticeably more stable before gliding into a landing.

The dramatic change in pitching moment with throttle setting was unexpected. Initially this effect was believed to be related to the thrust line not acting along the vertical CG. The aircraft's vertical CG was found, and the moment created by the thrust is equivalent to ~3° of nose up elevator, which should have been easily trimmable. To more accurately determine the power effects a wind tunnel test was completed with a propulsion system, and the results were discussed in section 6.6. The results indicate that the aircraft stability is strongly dependent on the throttle, with full throttle reducing the SM by ~6%. This reduction is static margin also means that at large angles of attack the change in moment would require more than 10° of elevator to trim, as shown in Figure 53.

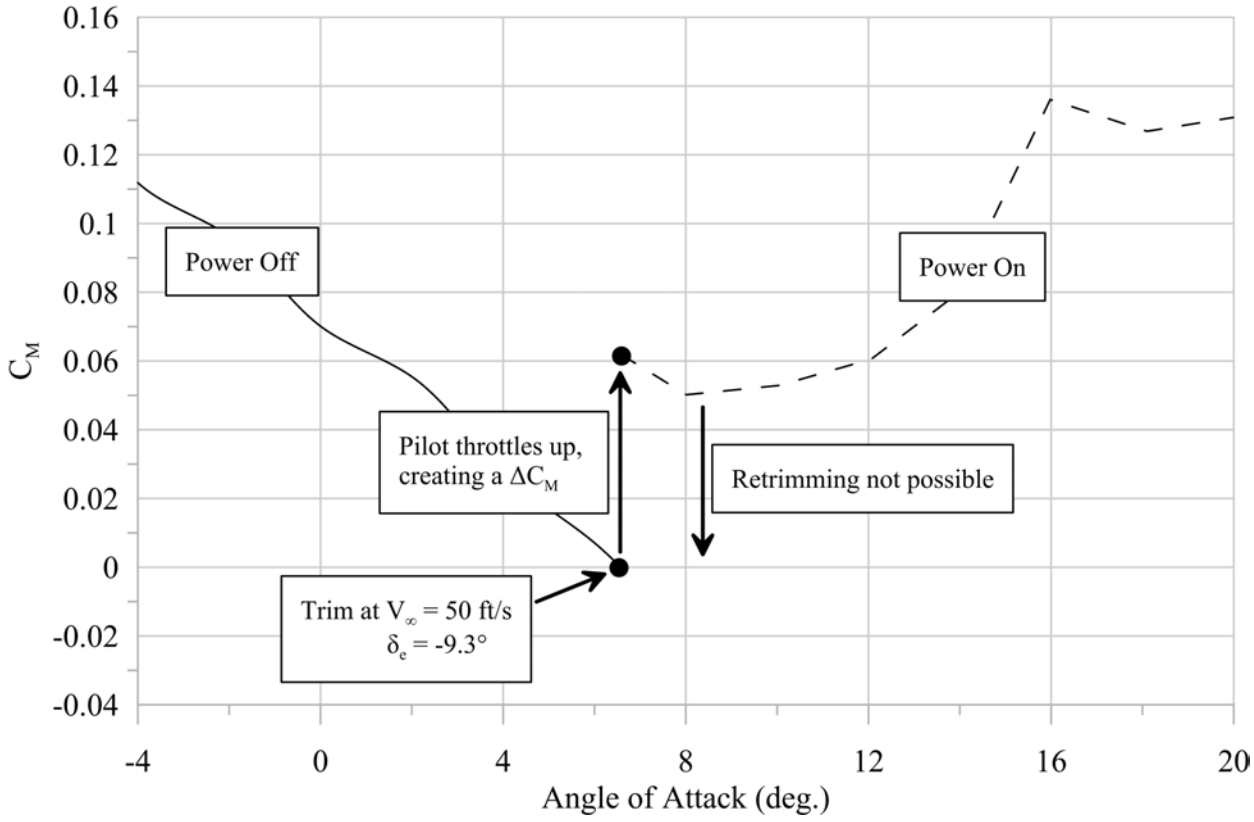

Figure 53. Change in aircraft pitching moment after throttling up.

To counteract this effect the motor was mounted with 3° of nose down tilt, which creates the equivalent of 10° of nose down elevator. Although this should fix the issue, the pilot felt that in flight it would be difficult to react quickly enough to maintain stability. To assist the pilot in keeping the aircraft safe a stability augmentation system (SAS) was added. The system selected was the FrSky S series of receivers [23], which contain a built-in SAS. This system is lightweight, simple to setup, and was the same size of the receiver originally selected. Several modes are selectable but auto-level, which attempts to maintain the aircraft level in both roll and pitch was used for all testing.

Flights were then made after the SAS was added and the motor was tilted down. In order to successfully launch the pilot had to throttle up slowly and could only make small elevator inputs.

If even moderate inputs were made the aircraft would become unstable and tumble. The pilot only flew at about 25% throttle, which resulted in a lower airspeed than anticipated. This required a larger elevator deflection to trim than expected, and small inputs from the pilot pushed this over the limit into an unstable angle of attack, as shown in Figure 54.

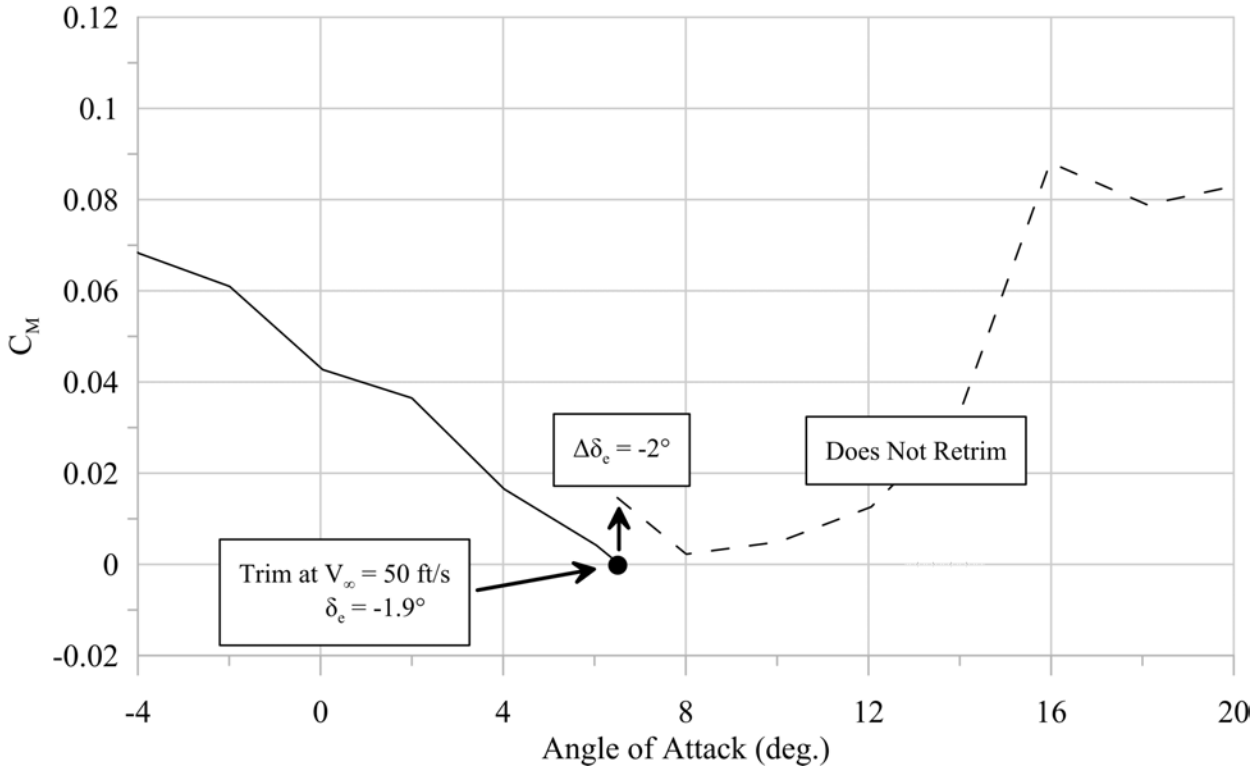

Figure 54. Impact of nose down tilt and elevator deflection on pitching moment.

To improve performance and reduce the risk of stall vehicle changes were made. First, the aircraft weight was reduced by removing the weight of a planned data acquisition system. This reduced the weight by 0.2 lbs, to 1.42 lbs, a 12.5% reduction. Second, the CG location was shifted forward to 36.5% to compensate for the reduction in SM due to power effects. Third, wing fences, which were discussed in section 6.3.2, are added to the aircraft to limit the risk of stall. Finally the pilot was instructed to fly at a higher speed than previous flights by increasing the throttle to 50%. These changes result in the aircraft being more stable, and trimming at a lower C_L in cruise,

keeping the aircraft further away from the unstable condition. The effect of these changes on pitching moment are shown in Figure 55.

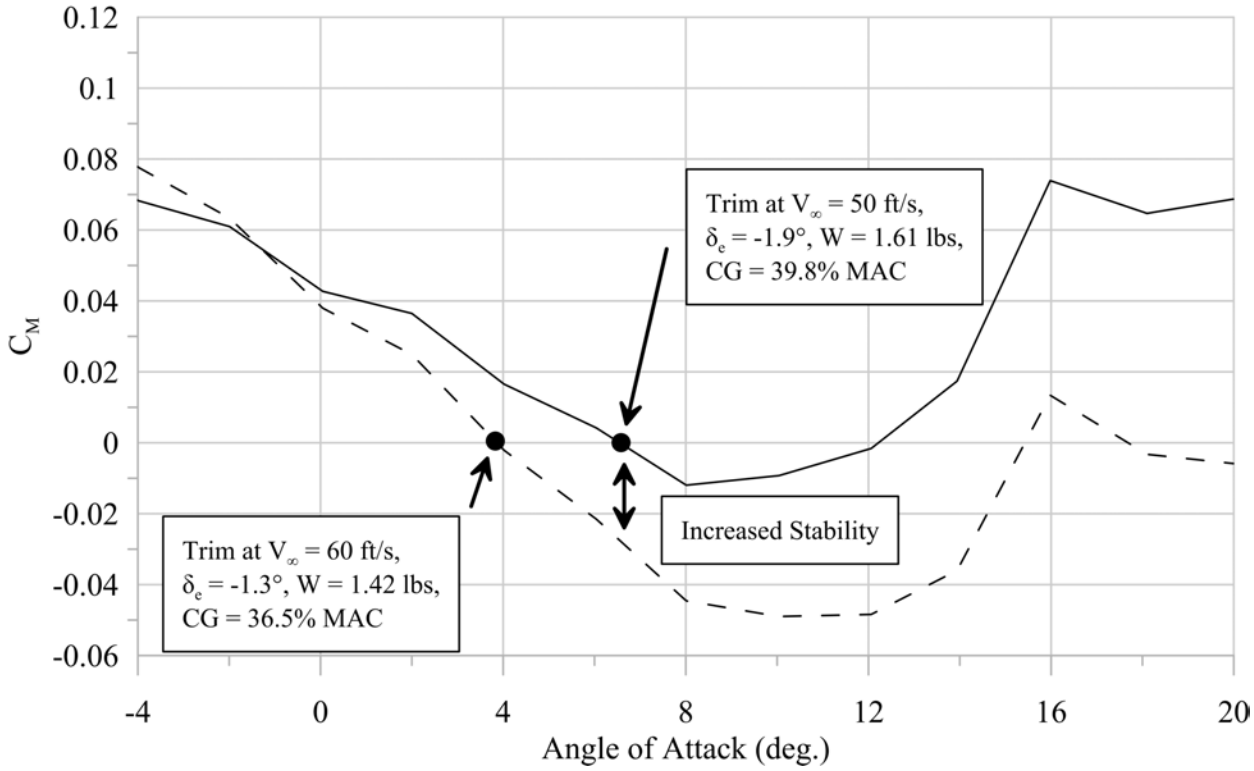

Figure 55. Pitching moment after vehicle changes.

After making these changes the model was flown and showed much improved performance and stability. With these changes it was even possible to fly the aircraft with no SAS, including the bungee launch. The pilot preferred the aircraft with no SAS, and even felt comfortable enough with the aircraft to perform barrel rolls and other aggressive maneuvers.

Upon completion of several successful flights the vertical tail was removed from the baseline to see if there was sufficient yaw stability using only the stabilizer. Several attempts at launching the aircraft were made, with none being successful. As soon as the aircraft would release from the bungee it would yaw significantly and then the pilot would lose control. This shows as was expected additional vertical surface is required to maintain stability and control.

7.2 Variable Cant Longitudinal Control

Flying the baseline aircraft provided a lot of information as to how the aircraft behaved, and what precautions should be taken to prevent stall. These lessons were applied to the variable cant configuration to ensure a successful flight on the first attempt. A maximum stabilizer cant of 60° was chosen for the test flight. A larger cant angle would provide a larger trim C_L, but there is also a greater risk of stalling. The CG location is set at 13.2% MAC so that at the 60° cant angle the SM is 16%. The flaperons are also set to -7.5°, which increases the trim C_L. The stabilizer incidence angle was set to 5° to reduce the minimum trimmable C_L.

Upon bungee launch the aircraft impacted the ground and as a result of the impact the fuselage aerodynamic cover fell off. The aircraft was able to continue flying, but the loss of the cover likely resulted in a much larger drag, and a loss of lift on the wing center portion. The loss of lift at the wing center would have shifted the NP aft, resulting in increased stability and a lower trimmable C_{Lmax}. The pilot reported having to use large nose up elevator input to trim the aircraft at cruise, which was likely caused by these effects from the fuselage cover falling off. He also reported that the aircraft was “sluggish” in pitch which is due to the large static margins at small cant angles.

7.3 Handling Qualities

After test flying completion the pilot was asked to rate the aircraft’s handling qualities. The Cooper-Harper Rating system was used [24]. Pilots use the tool to rate handling qualities of aircraft, with 1 being the best and 10 being the worse. The results for the various aircraft are shown in Table 6.

TABLE 6

COOPER-HARPER RATINGS FOR VARIOUS CONFIGURATIONS

Configuration	Rating
Baseline with SAS	9
Baseline No SAS	5-6
Variable Cant – Pitch Control	7

CHAPTER 8

CONCLUSION

The goal was to determine if the B&V semi-tailless concept is viable for small UAVs, and if the variable cant stabilizer is viable for aircraft control. A combination of analytic methods and vortex lattice solvers were used to analyze the configurations and identify key parameters for control and trim. Models were then constructed to validate predictions. Wind tunnel testing validated longitudinal forces and moments, with a focus on stability, control, and performance. Flight testing was then performed to provide feedback on the handling qualities. A results summary related to these goals is presented:

- The Blohm & Voss semi-tailless concept, with the addition of vertical area, is valid for small UAVs and can be made stable and controllable.
- The variable cant stabilizers can be used to control and trim the aircraft longitudinally. However, the variable cant stabilizers are likely not suited to controlling the aircraft lateral-directionally, and also not likely suited to controlling the aircraft longitudinally and lateral-directionally simultaneously.
- No significant benefits in performance were found for the variable cant stabilizers compared to the baseline configuration but may be possible with optimization.

CHAPTER 9

RECOMMENDATIONS FOR FUTURE WORK

This thesis demonstrated that the B&V semi-tailless concept is valid for small UAVs, and the variable cant configuration is viable. More work should be done, and the following recommendations are made for future work:

- Eliminating the tip stall: Study methods for eliminating tip stall. Washout could be used with minimal increase in drag.
- Design optimization: Using the studied B&V aircraft as a starting point optimize the aircraft design for small UAVs to fit specific mission requirements. A more detailed analysis of required vertical area and shifting vertical tails to the wing tips is appropriate, as is minimizing fuselage wetted area.
- Optimization of variable cant configuration for pitch control: The effect of stabilizer size was not included in this study. This aspect should be investigated to determine the optimum size for trim and performance. A reflexed airfoil could be used on the main wing to get desired pitching moment characteristics and reduce drag.
- Design of a non-linear controller: The variable cant configurations provide non-linear control. A non-linear controller could be designed to improve the aircraft handling qualities.
- Wing tip mounted motors: A study on mounting two motors on the wing tip rather than a single motor in the center of the aircraft. This could free up the middle of the aircraft for sensors or other payloads without being affected by the motor/propeller. These motors could also be used for active yaw control, eliminating the need for a vertical tail.

Power effects would have a large impact on control but would make the aircraft more stable.

- Forward swept semi-tailless configuration: Application of the semi-tailless concept to a forward swept wing. The stabilizers could be mounted forward of the wing leading edge, at a fixed cant angle, and trailing edge control surfaces used for control.

REFERENCES

REFERENCES

[1] Bill, R., *Secret Projects: Flying Wings and Tailless Aircraft,* Ian Allen Publishing, Hersham, England, 2010, pp. 37-39.

[2] Meyer, I. and Walter, S., *Luftwaffe Secret Projects – Fighters 1939-1945,* Midland Publishing, Leicester, England, 1997, pp. 32-33.

[3] "Blohm & Voss P 208," Luftfahrt International, vol. 15. Pp. 2325-2339, May – June 1976.

[4] Kentfield, J.A.C., "Aircraft with outboard horizontal stabilizers, history, current status, development potential," *Progress in Aerospace Science,* vol. 45, 2009, pp. 169-202.

[5] Tipton, B., "The preliminary design analysis of a unique semi-tailless aircraft configuration," MSc Dissertation, University of Oklahoma, Norman, Ok, 1995.

[6] Muller, K. W., "Analysis of a semi-tailless aircraft design," MSc Dissertation, US Navy Post-Graduate School, Monterey, California, 2002.

[7] Bourdin, P., Gatto, A., and Friswell, M., "The Application of Variable Cant Angle Winglets for Morphing Aircraft Control," *24th AIAA Applied Aerodynamics Conference,* 2006.

[8] Bourdin, P., Gatto, A., and Friswell, M. I., "Aircraft Control via Variable Cant-Angle Winglets," *Journal of Aircraft*, vol. 45, 2008, pp. 414–423.

[9] Gatto, A., Bourdin, P., and Friswell, M. I., "Experimental Investigation into Articulated Winglet Effects on Flying Wing Surface Pressure Aerodynamics," *Journal of Aircraft*, vol. 47, 2010, pp. 1811–1815.

[10] Bourdin, P., Gatto, A., and Friswell, M., "Potential of Articulated Split Wingtips for Morphing-Based Control of a Flying Wing," *25th AIAA Applied Aerodynamics Conference*, 2007.

[11] Raymer, D. P., *Aircraft design: a conceptual approach*, 5th ed., AIAA, Reston, VA, 2018. pp. 610-613.

[12] OpenVSP, Open Vehicle Sketch Pad, Software Package, Ver. 3.16.1, NASA, 2018

[13] Hahn, A., "Vehicle Sketch Pad: A Parametric Geometry Modeler for Conceptual Aircraft Design," *48th AIAA Aerospace Sciences Meeting Including the New Horizons Forum and Aerospace Exposition*, 2010.

[14] Nicolai, L., "Estimating R/C Model Aerodynamics and Performance," URL: https://www.google.com/url?sa=t&rct=j&q=&esrc=s&source=web&cd=3&ved=2ahUKEwjw0vXchtvgAhUIiqwKHbiADuwQFjACegQICBAC&url=http%3A%2F%2Fstudents.sae.org%2Fcompetitions%2Faerodesign%2Frules%2Faero_nicolai.doc&usg=AOvVaw1LGlaI2QR7sEypiAClQecj [Retrieved 26 February 2018].

[15] Rae, W. H., Pope, A., and Barlow, J. B., *Low-Speed Wind Tunnel Testing*, 3rd ed., John Wiley & Sons, New York, 1999. pp. 65.

[16] Raymer, D. P., *Aircraft design: a conceptual approach*, 5th ed., AIAA, Reston, VA, 2018. pp. 127.

[17] Jacobs, E. N., Sherman, A., "Airfoil Section Characteristics as Affected by Variations of the Reynolds Number," NACA Report No. 586, Jan. 1937.

[18] Raymer, D. P., *Aircraft design: a conceptual approach*, 5th ed., AIAA, Reston, VA, 2018. pp. 160.

[19] Roskam, J., *Aircraft Design Part VI: Preliminary Calculation of Aerodynamic, Thrust and Power Characteristics,* DARcorporation, Lawrence, KS, 1984, pp. 82.

[20] Bandettini, A., Selan, R., "The Effects of Leading-Edge Extensions, A Trailing-Edge Extension, and A Fence on the Static Longitudinal Stability of a Wing-Fuselage-Tail Combination Having a Wing with 35° of Sweepback and an Aspect Ratio of 4.5," NACA Research Memorandum A53E12, Aug. 1953.

[21] Lennon, A., *The Basics of R/C Model Aircraft Design*, Air Age Inc, Wilton, CT, 1996. pp. 69-71, 96.

[22] Rae, W. H., Pope, A., and Barlow, J. B., *Low-Speed Wind Tunnel Testing*, 3rd ed., John Wiley & Sons, New York, 1999. pp. 307-313.

[23] URL: https://www.frsky-rc.com/product-category/receivers/s-series/, accessed March 31, 2019.

[24] Cooper, G. E., Harper, Jr., R. P., "The Use of Pilot Rating in the Evaluation of Aircraft Handling Qualities," NASA TN D-5153, April 1969.